

## Age and depositional environment of the Xiaheyuan insect fauna, embedded in marine black shales (Early Pennsylvanian, China)

Steffen Trümper<sup>a,b,\*</sup>, Jörg W. Schneider<sup>b,c</sup>, Tamara Nemyrovskaya<sup>d</sup>, Dieter Korn<sup>e</sup>, Ulf Linnemann<sup>f</sup>, Dong Ren<sup>g,\*</sup>, Olivier Béthoux<sup>h,i</sup>

<sup>a</sup> Museum für Naturkunde Chemnitz, Moritzstraße 20, D-09111, Chemnitz, Germany

<sup>b</sup> TU Bergakademie Freiberg, Institut für Geologie, Bernhard-von-Cotta-Straße 2, D-09596, Freiberg, Germany

<sup>c</sup> Kazan Federal University, Institute of Geology and Petroleum Technologies, Kremlyovskaya 18, 420008, Kazan, Russia

<sup>d</sup> Institute of Geological Sciences, National Academy of Sciences of Ukraine, O. Gonchar Street 55-b, 01601, Kiev, Ukraine

<sup>e</sup> Museum für Naturkunde der Humboldt-Universität zu Berlin, Invalidenstraße 43, 10115, Berlin, Germany

<sup>f</sup> Senckenberg Naturhistorische Sammlungen Dresden, Museum für Mineralogie und Geologie, Sektion Geochronologie, Königsbrücker Landstraße 159, D-01109, Dresden, Germany

<sup>g</sup> College of Life Science, Capital Normal University, Beijing, 100048, China

<sup>h</sup> CR2P (Centre de Recherche en Paléontologie – Paris), MNHN – CNRS – Sorbonne Université, Paris, France

<sup>i</sup> Muséum National d'Histoire Naturelle, 57 rue Cuvier, CP38, F-75005, Paris, France

### ARTICLE INFO

#### Keywords:

Taphonomy  
Late Carboniferous  
Conodonts  
Ammonoids  
U–Pb dating  
Interdelta bay

### ABSTRACT

The Early Pennsylvanian Xiaheyuan entomofauna (Ningxia, China) is among the earliest assemblages of winged insects known so far, and therefore provides an essential input on deciphering the early diversification of this group. Despite its evolutionary significance, both the age and depositional environment remained poorly constrained. Here, we present high-resolution documentation of litho- and biofacies, biostratigraphy and geochronology of the up to 100 m thick type section. Accordingly, the insect-bearing strata are of latest Bashkirian (latest Duckmantian) to middle Moscovian (Bolsovian) age. The sediments, lithostratigraphically assigned to the Yanghugou Fm., represent a regression marine sequence formed at the southern margin of the Qilian Inland Sea. Intercalations of crevasse channels and splays that laterally interlock with marine black shales and bioclastic limestones point to deposition in an interdelta bay. Ground-touching waves provoked the erosion of muds at shallow depths leading to mass mortalities among mollusc communities due to rising anoxia, turbidity and water turbulence. In addition, bottom currents transported mud intraclasts towards the basin, where sinking insects that reached the bay via winds and surface currents were buried sub-contemporaneously with bivalves below the storm wave base. Observed differences in insect preservation and assemblage composition across the sequence are found to correlate with lithology and are best explained by distance from land, and the action of events inducing insect carcasses to sink, such as storms. The proposed taphonomic model represents a new fossilization pathway from land to sea and provides new directions for prospecting Paleozoic deposits in the search for insects.

### 1. Introduction

Terrestrial ecosystems of the Carboniferous were characterized by an unprecedented diversity of arthropods (Dunlop, 2010; Shear and Edgecombe, 2010; Wolfe et al., 2016). As for winged insects, they make an apparent sudden appearance in the Late Mississippian (Brauckmann and Schneider, 1996; Petrulevičius and Gutiérrez, 2016). But it is not until the Early Pennsylvanian that a few suitable outcrops, such as Hagen-Vorhalle (Germany), Mazon Creek (USA) and Commeny

(France) yield diverse assemblages of winged insects (Brongniart, 1893; Carpenter, 1997; Brauckmann et al., 2003). Considering the occurrence of wingless hexapods in the Devonian, the 35-million-years-long gap is most likely due to a lack of suitable outcrops. As a consequence, Early Pennsylvanian localities providing insects are of utmost importance for our understanding of the early diversification of the group.

About two decades ago fossil insects were mentioned by Hong and Peng (1995) at the Pennsylvanian Xiaheyuan locality. In the last six years, this North Chinese locality was subjected to intensive excavation.

\* Corresponding author.

\*\* Corresponding author. Museum für Naturkunde Chemnitz, Moritzstraße 20, D-09111, Chemnitz, Germany  
E-mail address: [rendong@cnu.edu.cn](mailto:rendong@cnu.edu.cn) (D. Ren).

<https://doi.org/10.1016/j.palaeo.2019.109444>

Received 27 January 2019; Received in revised form 13 October 2019; Accepted 1 November 2019

Available online 13 November 2019

0031-0182/ © 2019 Elsevier B.V. All rights reserved.

The description of the insect content is ongoing, but it can already be assessed that at least seven insect orders are present, with stem-relatives of Orthoptera (grasshoppers, crickets and katydids) dominating in terms of abundance and number of species (Prokop and Ren, 2007; Béthoux et al., 2011; Béthoux et al., 2012a,b; Li et al., 2013a,b; Wei et al., 2013; Pecharová et al., 2015; among others). Besides this remarkable diversity, the collected material is abundant, allowing solid inferences on wing venation intra-specific variability in various lineages (Béthoux et al., 2011, 2012b; Cui et al., 2011; Gu et al., 2011; Li et al., 2013; Pecharová et al., 2015), and the identification of both males and females for some species (Pecharová et al., 2015; Du et al., 2016). Moreover, the sediment preserved minute sensory structures of the insects (Prokop et al., 2016). Particularly unusual among insect-bearing Paleozoic localities is the occurrence in a thick marine black-shale succession providing abundant ammonoids and bivalves (Lu et al., 2002). Finally, insect assemblages occur in distinct layers, and it has already been shown that their composition and the state of preservation of the contained insects vary across the section (Robin et al., 2016).

However, further progress in the investigation of the Xiaheyuan entomofauna is impeded by three main obstacles. First, the sampled layers are not correlated, this situation precluding a proper analysis of lateral variations in insect assemblages. Second, both depositional environment and insect taphonomy are not understood with sufficient details, making comparisons between assemblages across the section, and with other Pennsylvanian localities, weakly informative. Finally, the age of the locality remains poorly constrained.

In order to address these issues, we carried out a detailed bed-by-bed documentation of the insect-bearing strata, including correlation between the sampled areas. In addition, based on lithofacies and biofacies analysis, a detailed interpretation of the depositional environment and insect taphonomy is proposed. The age of the locality is newly assessed based on multiple proxies.

## 2. Geological background

The study area is located at the foothills of the eastern North Qilian Mountains, 8 km southwest of Zhongwei, Ningxia Hui Autonomous Region, in Northwest China (Fig. 1A and B). Steeply inclining strata of Pennsylvanian to early Permian age are exposed along the Xiangshan-Tianjinshan Fault — a major regional fault by which the late Paleozoic strata have been overthrust on Cenozoic conglomerates since the Miocene (Fig. 1C; Zhang et al., 1990; Shi et al., 2015). Insect-bearing strata were considered of earliest Pennsylvanian (Namurian B/C) age based on ammonoids and conodonts (e.g., Lu et al., 2002). However, this stratigraphic affiliation remains highly controversial because of irreproducible profile documentations and a disputable regional lithostratigraphic subdivision of the Carboniferous (see Supplementary material 1).

The Ningxia region belongs to the western Sino-Korean Craton which, during the Carboniferous, was part of a tropical archipelago located at the eastern margin of the Paleo-Tethys (Fig. 2A; Nie, 1991; Wang and Pfefferkorn, 2013; Xiao et al., 2013). The Sino-Korean Craton was surrounded by passive continental margins against the Paleo-Tethys to the West and South and the Panthalassa Ocean to the East. To the North, an active andinotype volcanic arc probably marked the border to the Paleo-Asian Ocean (Shen et al., 2006; Zhang et al., 2007; Zheng et al., 2014). In relation to its paleogeographical position, Northern China underwent a tropical ever-wet climate favoring extensive coal formation from the Carboniferous until the late Permian (Liu, 1990; Cope et al., 2005). During Early Pennsylvanian times, the Ningxia region was captured by the epicontinental Qilian Basin, in which shallow marine, littoral and paralic sediments were deposited (Fig. 2B; Tong, 1993; Liu et al., 2014). According to Tong (1993) and Xie et al. (2004) the outline, internal structure and sedimentation of this basin were determined by reactivated faults.

## 3. Materials and methods

As a preliminary remark, materials used for lithological and geochronological analyses are stored with the inventory number FG-680 in the central sample archive (Lithothek) of the Technical University Bergakademie Freiberg, Germany. Insects used for taphonomy are housed at the Capital Normal University in Beijing/China. Each surveyed specimen is associated with a 'collect label' indicating its systematic identification, the author(s) of the identification, the name of the collector, the year of collect, and the excavation site it was recovered from. Specimens of particular importance were incorporated to the CNU-NX1 collection (together with their 'collect label'). If so, a twin of the 'collect label', on which the CNU-NX1 number is indicated, was kept together with the original, remaining sample.

### 3.1. Lithofacies analysis

During two field campaigns in 2014 and 2015 lithofacies, thicknesses, fossil content and taphonomy of four sections in non-disturbed areas of the Xiaheyuan locality were documented at a centimetric resolution. The sections are exposed in N-S-trending erosional gullies dissecting the foothills of the North Qilian Mountains (Fig. 1B). Three sections have a length of 100 m and one has a length of 300 m with the Xiangshan-Tianjinshan Fault as its base. Lateral distance between outermost sections reaches an extent of 770 m. Stratigraphic correlation rests upon marker horizons, i.e., ash layers, carbonates or black shales showing recognizable fossil contents, and the cyclic constitution of the sections. Lithofacies analysis follows the hierarchical concept proposed by Miall (1996) in a modified form. Accordingly, sediments are grouped into lithofacies types (LFT's) defined by their texture, bedding and fossil content. Each LFT is indicated by two letters: the first, capital letter accounts for the dominating grain size, while the second, small letter indicates the bedding (Table 1). Additionally, particular capital letters were applied in case of notable sedimentological features. Microfacies and petrography were characterized by means of 20 thin sections. The spatial arrangement of the LFT's is used to describe the lithofacies architectures of the Xiaheyuan profile.

### 3.2. Insect taphonomy

Insect assemblages have been collected from several excavation sites. Their names include the name of the corresponding section plus a consecutive number indicating the chronological order of opening [e.g. the assemblage 'Peacock 0' (Pe 0) was excavated earlier than assemblage 'Peacock 1' (Pe 1), both originating from Peacock Hill section]. Taphonomic analysis follows the procedure elaborated by one of us (OB) and described in Robin et al. (2016; suppl. data). We complemented data from these authors with 166 specimens from two sites, namely Peacock 2 and Dragon 4.

### 3.3. Biostratigraphy and geochronology

Two fossiliferous limestone horizons were sampled and processed with 10% formic acid to extract conodont material. In addition, two out of four ash layers were sampled to obtain U–Pb ages from zircons. Zircons were analyzed for U, Th, and Pb isotopes by Laser Ablation and Inductively Coupled Plasma Mass Spectrometry (LA-ICP-MS) at the GeoPlasma Lab, Senckenberg Naturhistorische Sammlungen Dresden, using a Thermo-Scientific Element 2 XR sector field ICP-MS coupled to a RESOLUTION Excimer Laser System (193 nm). For further detail on geochronology, see Supplementary material 2.

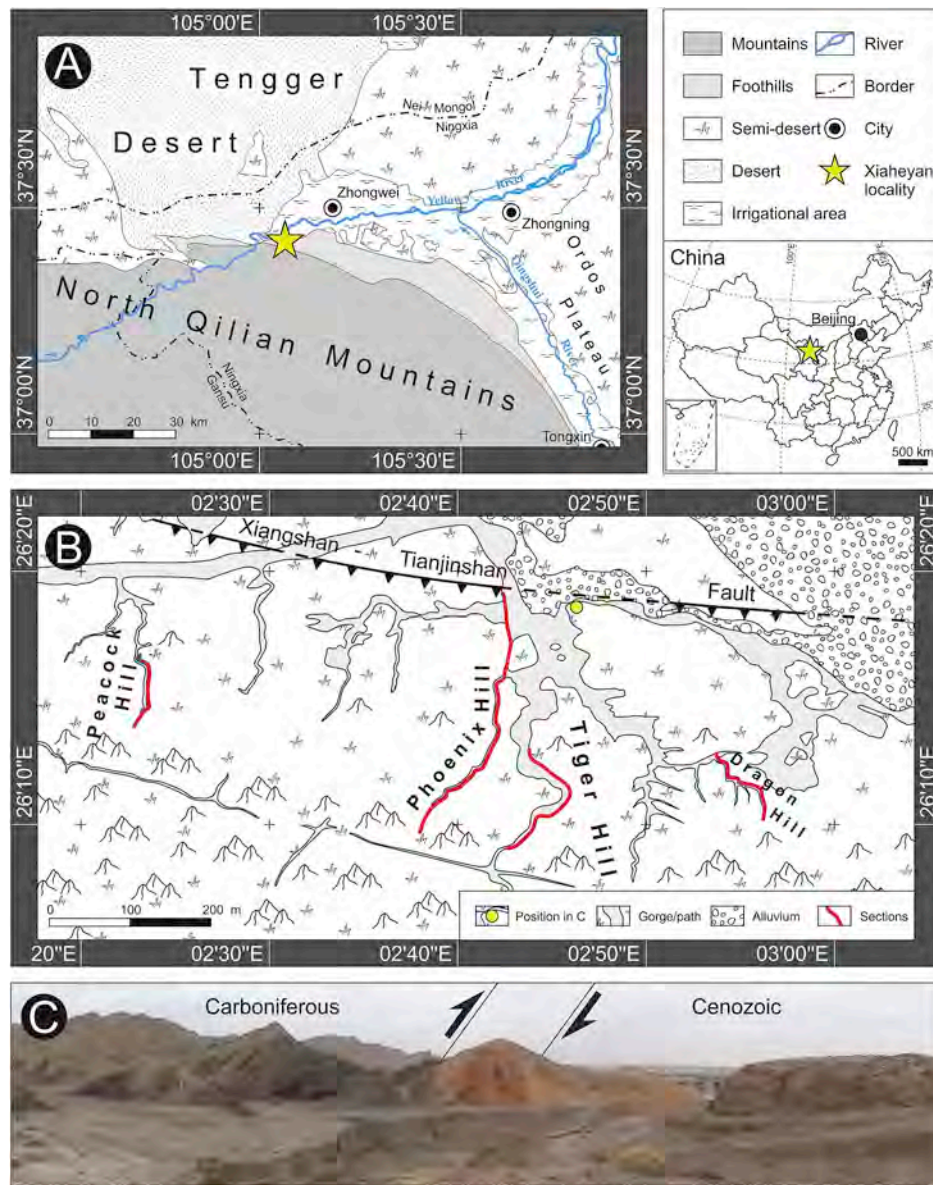


Fig. 1. Xiaheyuan locality. (A, B) Position of the study area in the Ningxia Province (China). (C) View at the Xiangshan-Tianjinshan Fault, which separates steeply inclining Carboniferous strata in the south from horizontal Cenozoic conglomerates in the north.

## 4. Results

### 4.1. Lithofacies types

Generally, the Xiaheyuan sections are composed of two facies: a prevailing black shale facies with subordinate carbonates and a clastic non-shale facies. Whereas the clastic non-shale LFT's are summarized in Table 2 and Fig. 3, the insect-bearing black shale facies is described in detail in the following.

Four LFT's can be distinguished within the black shale facies. One is dominated by horizontal lamination (LFT Bh), two show a fabric referred to as lenticular lamination (O'Brian and Slatt, 1990; Schieber et al., 2010, Fig. 4A and B), and one is massive (LFT Bm). Focusing on lenticular lamination, the fabric consists of an accumulation of (sub-) mm-scale ellipsoidal mud aggregates, each exhibiting a lenticular to irregular shape in vertical sections (Figs. 4A and B). Lenticularly laminated LFT's differ in size of the mud intraclasts and include intercalations of 1 mm thick, non-stratified siltstone layers, delimited by sharp lower and upper boundaries (Fig. 4C). Micro cross-lamination is rarely evident (Figs. 4C and D). Up to 300  $\mu$ m large angular to rounded

quartz grains can occur (Fig. 4E). Around quartz grains as well as shell remains, the sediment is differentially compacted (Figs. 4E and F).

#### 4.1.1. LFT Bh: horizontally laminated black shale (Fig. 4G and H)

Black shales of LFT Bh possess horizontal bedding that consists of 250–300  $\mu$ m thick horizontal laminae showing sharp boundaries (Figs. 4G and H). In a vertical direction, laminae may change in their internal structure, ranging from laminae transitional to LFT Bl<sub>2</sub> to laminae showing inverse grading (both shown in Fig. 4G). Intercalations of LFT Bl<sub>2</sub> layers are common. Fossils are extremely rare, including insect remains, the bivalve *Posidoniella de Koninck, 1885*, indeterminate juvenile molluscs and plants. Among the latter, highly macerated fragments as well as up to 10 cm large lycopsid stems, sphenopsid and pteridosperm foliages were found.

#### 4.1.2. LFT Bl<sub>1</sub>: lenticularly laminated black shale 1 (Fig. 5)

This macroscopically light greyish LFT consists of tightly packed mud aggregates ranging in size from 75 to 170  $\mu$ m in vertical diameter, and from 250 to 1500  $\mu$ m in horizontal diameter (Fig. 5A). The fossil content is dominated by low-diversity bivalve mass assemblages,



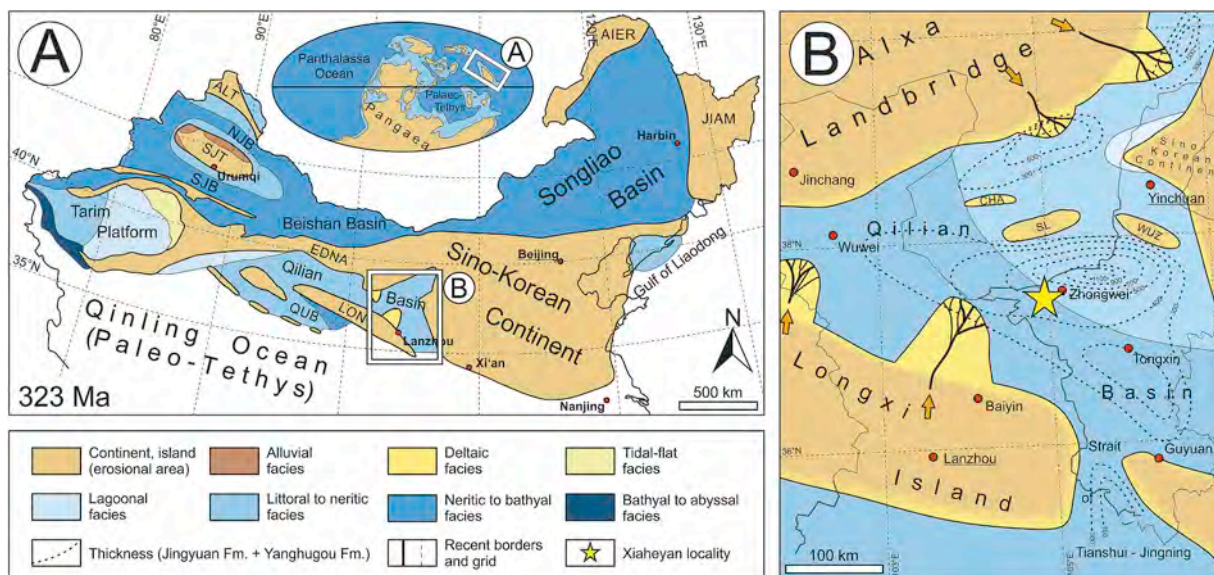


**Fig. 2.** Paleogeography of Northern China (A) and Ningxia (B) around the Mississippian-Pennsylvanian boundary. Compiled and modified after Tong and Li (1994), Ruan (1996), Zhu et al. (2007) and Yan et al. (2008). Abbreviations: AIER: Aierguna Island; ALT: Altai Island; EDNA: East Tarim-Dunhuang-North Qilian-Alxa Land bridge; JIAM: Jiamusi Island; LON: Longxi Island; NJB: North Junggar Basin; QUB: Quaidam Basin; SJB: South Junggar Basin; SJT: South-Junggar-Tuha Island.

**Table 1**  
Symbology used for lithofacies analysis.

Grain size	Bedding	Special symbols
G Gravel	b lenticularly bedded	B Black shale
S Sand	g graded	C Coaly mud
F Fine-clastics	h horizontally bedded	L Limestone
	l lenticularly laminated	R Rooted siltstone
	m massive	
	r ripple-cross bedded	
	t trough-cross bedded	

**Table 2**  
Non-shale lithofacies types.

Facies code	Facies description (incl. figure reference)	Interpretation
C	Black, coaly mudstones with faint horizontal bedding and tiny plant remains. Occurs rarely and forms a few centimeters thick horizons (Fig. 3A).	Standing water body with high accumulation rate of organic matter.
R	Greyish brown siltstones with indistinct horizontal bedding. Subhorizontally penetrated by abundant, 2–6 mm thick roots resembling lycopsid appendices, which may increase in size towards the top (Fig. 3B).	Autochthonous incipient root soil.
Fh	Brown siltstones with horizontal bedding. Bedding planes are covered by mica and tiny plant remains preserved as compressions. Rare intercalations of dense accumulations of up to 10 cm large lycopsid stems and pteridophyte fronds (Fig. 3C).	Subaquatic deposition at low-energetic, unidirectional flow conditions.
Sb	Greyish white fine- to medium-grained silty sandstones with lenticular bedding. Primary fabric often obliterated by soft-sediment deformation (Fig. 3D).	Subaquatic deposition at fluctuating low-energetic, unidirectional flow conditions.
Sr	Greyish yellow fine- to medium-grained sandstones with ripple-cross bedding on a 0,5 cm-scale (Fig. 3E).	Subaquatic deposition of the lower flow regime.
Sh	Greyish white well-sorted fine-grained sandstones showing horizontal lamination on a mm-scale (Fig. 3F).	Subaquatic deposition at high stream velocities (upper plane bed).
St	Grey, pebbly, moderate- to coarse-grained sandstones showing small- to medium-scaled through-cross bedding (i. e. sets of less than 20 cm in thickness) (Fig. 3G).	Subaquatic dunes of the lower flow regime.
Sg	Poorly sorted, pebbly fine- to medium-grained sandstones with a sharp erosional base. Pebble fraction consists of rounded to subrounded quartz and irregularly shaped, often flattened black shale clasts at maximum diameters of 4 cm. The black shale clasts are orientated subhorizontally and decrease in size and abundance towards the top of lithofacies type Sg reflecting a normal grading. Occurrence of coalified, tiny plant remains (Fig. 3H).	Event-like deposition of hyperconcentrated to mass flows including the reworking of still plastic black shales.
Sm	Poorly sorted, pebbly fine- to coarse-grained massive sandstones. Quartz grains rounded to subrounded. Base and top are uneven, but sharp (Fig. 3I).	Subaquatic mass flow events.
Gm	Non-stratified, sandy, fine-grained conglomerates. Matrix cemented by calcite with (sub) angular grains. Pebble fraction rounded to subrounded. High compositional maturity with quartz as only component (Fig. 11J).	Highly energetic, subaquatic mass flows.

including complete juvenile and adult specimens, lacking orientation and sorting (Fig. 5B). Butterfly preservation remains an exception. Instead, most specimens have their valves still occluded. The shell beds mainly consist of *Posidoniella* (Fig. 5C), reaching a maximum size of 5 cm, followed by *Dunbarella Newell, 1938* (Fig. 5D). Adult *Euchondria Meek, 1874* (Fig. 5E) and assemblages exclusively composed of mytiloids (Fig. 5G) occur sparsely. Cm-scale plant remains can be surrounded by sparse to dense accumulations of juvenile *Posidoniella* individuals (Fig. 5F). In this case, most individuals have their umbo orientated towards the plant – often with the umbo in connection with



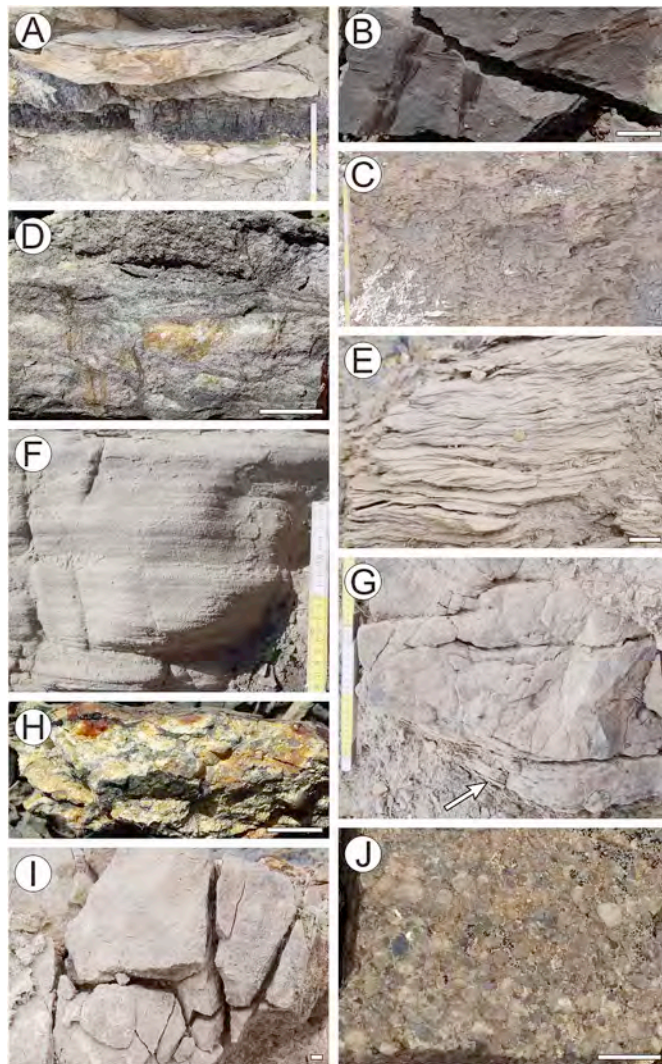


**Fig. 3.** LFT's of the non-shale facies. Scale: 1 cm. (A) LFT C represented by a coal seam underlain by a rooted soil and overlain by trough-cross bedded sandstones. (B) LFT R with lycopsid appendices on a bedding plane in siltstones. (C) LFT Fh. (D) LFT Sl. (E) LFT Sr. (F) LFT Sh. (G) LFT St. Note incision into underlying fine-clastics (arrow). (H) LFT Sg. (I) LFT Sm. (J) LFT Gm.

the plant itself. Some bedding planes display patchy accumulations of up to 3 mm large juvenile molluscs, displaying a discoid shape and a central cavity (Fig. 5H). Further relevant fossils are fragmentarily to completely preserved ammonoids (Fig. 5I), at least 3 cm long orthocone nautilids preserved as molds (Fig. 5J), a teallicaridid crustacean (*Laeviteallicaris xiaheyanensis* Yang et al., 2018), insect remains and fish scales. Plant fossils comprise lycopsid and sphenopsid foliages (*Lepidophylloides* Snigirevskaya, 1958, *Sphenophyllum* Brongniart, 1828, Fig. 5K, *Annularia* Sternberg, 1821), stems, single neuropterid leaflets, and plant fragments too incomplete and/or poorly preserved for proper systematic identification.

#### 4.1.3. LFT Bl<sub>2</sub>: lenticularly laminated black shale 2 (Fig. 4B)

On exposed surfaces, the greyish LFT Bl<sub>2</sub> is covered by secondarily formed jarosite and oxyhydroxides (Odin et al., 2018). Internally, tightly packed mud aggregates reach vertical diameters of 90–500 μm, as opposed to horizontal diameters of 500 μm to a couple of mm (Fig. 4A). The fossil content in general is identical to that of LFT Bl<sub>1</sub>, although it lacks mass occurrences of shells. Assemblages are characterized by sparse but more balanced accumulations of bivalves (*Posidoniella*, *Dunbarella*), complete and fragmentary ammonoids, juvenile

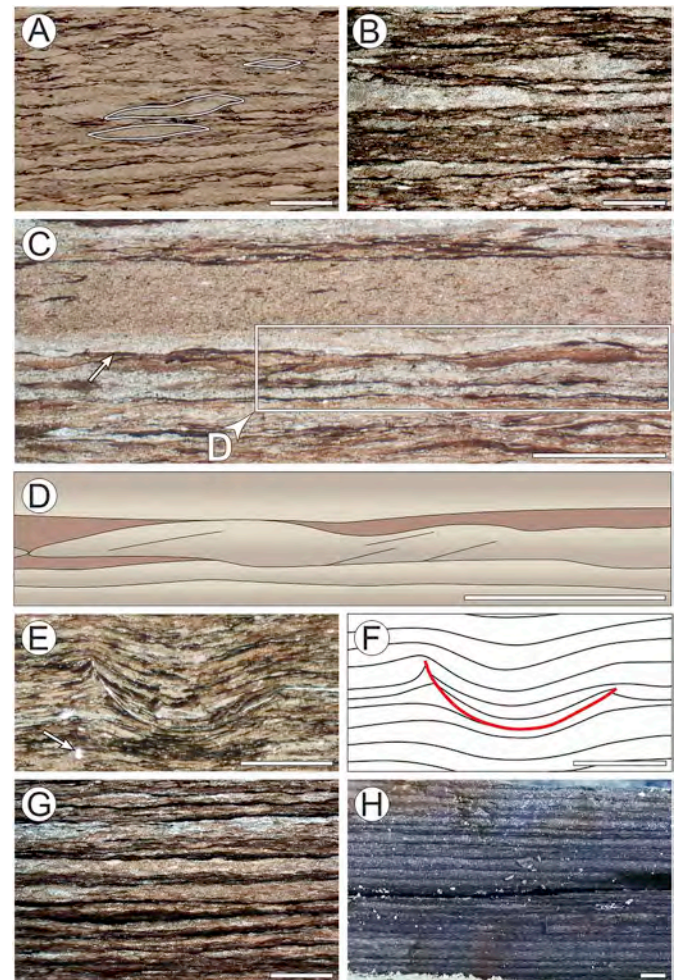


**Fig. 4.** Black shale microfabrics. Scale: 1000 μm. (A, B) Lenticular shape of mud aggregates (lines) in sections vertical to bedding. (C) Intercalation of a non-stratified siltstone layer, interpreted as distal turbidity current deposit. Note sharp boundaries (arrow). (D) Schematic close-up of C showing micro-cross stratification. (E, F) Differential compaction around a shell (red line in D). Note detrital quartz (arrow). (G, H) Microfacies (cross-cut) of LFT Bh. Note the distinct horizontal lamination. (For interpretation of the references to color in this figure legend, the reader is referred to the Web version of this article.)

molluscs, insects and plant fragments. Monospecific accumulations are rare and dominated by bivalves. In contrast to LFT Bl<sub>1</sub>, plant remains are larger and more diverse, containing tiny fragments, sphenopsid and lycopsid stems and foliages, neuropterid leaflets, pteridosperm fronds and cordaitalean leaves.

#### 4.1.4. LFT Bm: massive black shale (Fig. 6)

This LFT represents pure to silty black-colored claystone accounting for approximately one half of each Dragon, Phoenix and Peacock Hill sections. Due to the almost uniform grain size, a lumpy breakage is more common than cleavage along the bedding planes. At a microscopic scale, dark homogeneous clay dominates, rarely interspersed with up to 50 μm thick silt aggregates (Fig. 6A). This LFT is commonly associated with calcite or siderite intercalations, decimeters to 6 m long and up to 50 cm thick, and arranged in distinct stratigraphic levels (Fig. 6B). Spacing of bedding planes in the enveloping claystones increases towards these carbonates (Fig. 6C), indicating an early diagenetic origin.

Horizons with *Planolites* Nicholson, 1873 sporadically occur (Fig. 6D). Fossils are rare and comprise strongly macerated plant remains and isolated neuropterid pinnulae, rare and partially articulated



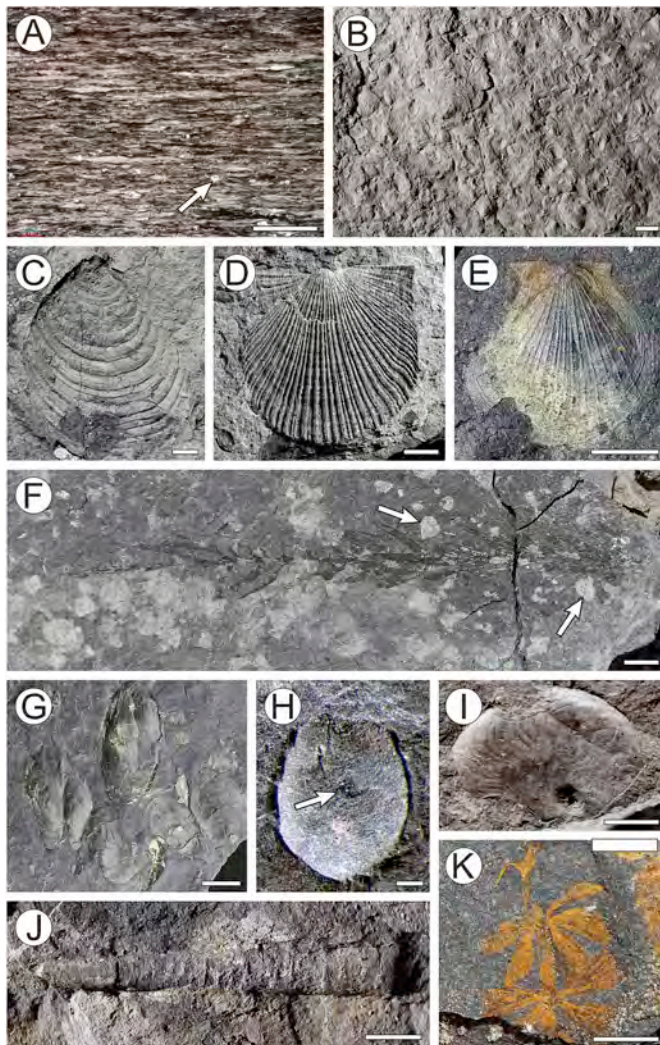


**Fig. 5.** LFT Bl<sub>1</sub>. (A) Microfacies (cross-cut). Note fine quartz sand grains (arrow). Scale: 1 mm. (B) Accumulation of juvenile *Posidoniella* shells on bedding plane. Note different sizes and the missing orientation of specimens. Scale: 5 mm. (C) *Posidoniella de Koninck*, (1885). Scale: 5 mm. (D) *Dunbarella Newell*, (1938). Scale: 5 mm. (E) *Aviculopecten McCoy*, (1851). Scale: 5 mm. (F) Lycopid sprout accompanied by sparse and dense clusters of juvenile *Posidoniella* specimens. Note the orientation of the umbo towards the plant (arrows). (G) Mytiloid shells in butterfly preservation. Scale: 5 mm. (H) Close-up of indeterminate juvenile mollusc showing a central cavity (arrow). Scale: 2  $\mu$ m. (I) Ammonoid fragment. Scale: 5 mm. (J) Orthocone nautilid preserved as a mold. Scale: 5 mm. (K) *Sphenophyllum* sp., imprint coated with limonite. Scale: 5 mm.

to isolated remains of actinopterygiid fish, lingulid brachiopods (*Orbiculoidea d'Orbigny*, 1847, Fig. 6E) and bivalves (*Dunbarella*, *Posidoniella*). In places, mass occurrences of complete and fragmented juvenile and adult ammonoids together with sparse plant fragments occur (Fig. 6F). Siderite concretions rarely contain accumulations of tiny shells and gastropods (Fig. 6G). The fossil content of calcite concretions ranges from dense, up to 20 cm thick, monospecific accumulations of *Dunbarella* (Fig. 6H) to oligospecific, dispersed assemblages made up of ostracods, gastropods and ammonoids (in decreasing order of abundance).

#### 4.1.5. LFT Lg: graded to stratified limestone (Fig. 7)

This LFT forms up to 40 cm thick beds (Fig. 7A) that can be traced laterally across distances of at least 1 km. Microscopically, they range from mudstones to floatstones and packstones made up of peloids showing average grain sizes of 200  $\mu$ m (max. 625  $\mu$ m), coarse silt to

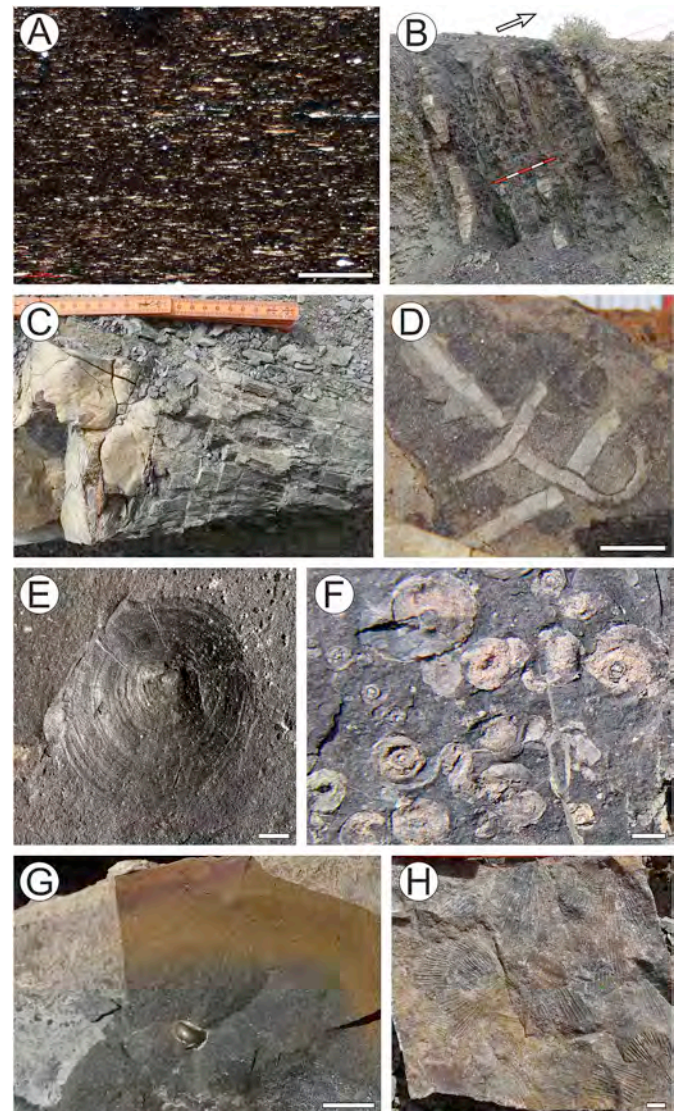


**Fig. 6.** LFT Bm. (A) Microfacies (cross-cut) showing rare silt aggregates in a claystone matrix. Scale: 1 mm. (B) Early diagenetic limestone concretions. Scale: 50 cm. The black arrow points to the top. (C) Close-up of B proving differential compaction of black shales. (D) *Planolites* tubes on bedding plane. Scale: 5 mm. (E) Lingulid brachiopod *Orbiculoidea d'Orbigny*, (1847). Scale: 1 mm. (F) Complete and fragmentary ammonoid tests of different ontogenetic stages on a bedding plane. Scale: 5 mm. (G) Gastropod whorl preserved as pyritized steinkern in a sideritic concretion. Scale: 5 mm. (H) Dense accumulation of *Dunbarella* on a bedding plane within a calcitic concretion. Scale: 5 mm.

sub-rounded quartz fine-sand and skeletal components (Figs. 7B and C). Fossils comprise ostracod valves, crinoid columnal segments, complete juvenile ammonoids and gastropods, isolated valves and tiny shell fragments in variable proportions. Beds of LFT Lg are subdivided into a lower unstratified part, with roughly aligned or nested components, and an upper part, bedded horizontally to wavy, in which components are orientated parallel to bedding (Figs. 7D and E). Horizontally aligned ostracod and mollusc valves occur both in convex-up and convex-down positions.

## 4.2. Section structure and facies architectures

### 4.2.1. Thickness and cyclicities

The 350 m thick Xiaheyuan section is subdivided into four units (Fig. 8; for legend see Fig. 9). The lower 90 m thick unit 1 consists of



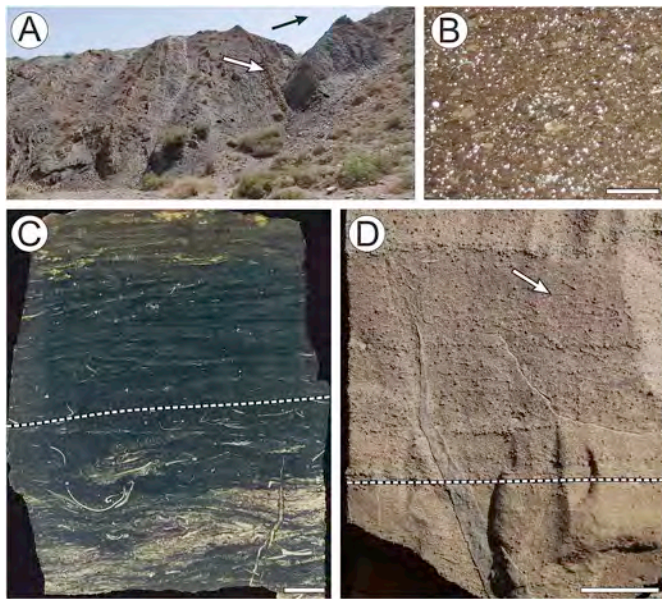


**Fig. 7.** LFT Lg. (A) Upper part of unit 3 at Tiger Hill (view towards East) revealing limestone banks (arrow). Black arrow pointing to the top. (B) Massive sandy pelmicrite at the base of LFT Lg. Scale: 1 mm. (C, D) Cross sections of LFT Lg. Note normal grading and horizontal alignment (arrow) of skeletal components and the transition (dashed line) from a lower, weakly stratified part to an upper, wavy or horizontally stratified part. Scale: 1 cm.

black shales and rare carbonates. It is overlain by the 80 m thick unit 2 containing black shales only (for detailed documentation see Supplementary material 3). Unit 3 has a thickness of 101 m at Dragon Hill and decreases westwards (86 m at Phoenix Hill, 78 m at Peacock Hill; Figs. 8 and 10). It begins with a coarse-clastic intercalation followed by black shales including carbonates and the insect-bearing strata. The section ends with the 80 m thick unit 4 composing of brown to pale siltstones and through-cross bedded sandstones.

The unit 3 displays repeated patterns indicative of a cyclic origin. Symmetrical and asymmetrical cycles of three orders were detected (Fig. 10). Third-order cycles are evidenced by the symmetric alternation of LFT Bm and laminated black shales (LFT's  $BL_1$ ,  $BL_2$ , Bh) on a 1- to 3-m scale. Transitions always remain gradual. Third-order cycles can be traced laterally across distances of at least 1 km.

In an upward direction, within third-order cycles, the proportion of laminated black shales increases at the expense of LFT Bm. This repetition composes the cyclicity of second order (Fig. 10). Accordingly, each of the 15–28 m thick second-order cycles typically begins with a thick LFT Bm unit (e.g., Dragon Hill, beds 49–51; Peacock Hill, beds 24–27; Fig. 10). Laminated black shales (LFT's  $BL_1$ ,  $BL_2$ , Bh), in contrast, dominate the upper part. Second-order cycles additionally reveal an upward-coarsening of black shale lamination, with LFT  $BL_1$  prevailing in the lower part and LFT  $BL_2$  characterizing the upper part of a cycle (Fig. 10). If present, LFT Bh typically forms the topmost bed of a second-order cycle.

Finally, an upward-increasing content and thickness of LFT Bh beds at the top of second-order cycles composes the first-order cyclicity (Fig. 10).

#### 4.2.2. Crevasse channels and splays

Crevasse channel elements occur in the basal part of unit 3 (Fig. 10), where they form lens-shaped, 10–150 m wide and less than 10 m thick bodies embedded in black shales of LFT Bm (Fig. 11A). Neighboring elements can be laterally connected by a thin sandstone layer made up of the LFTs Sl and Sh, or they are separated by black shales (Fig. 10E). Except for Peacock Hill, in which sandstones occur at a higher level (Fig. 10), crevasse elements are arranged in the same stratigraphic level at Dragon, Tiger and Phoenix hills. These deposits occur at the top of second-order cycles (Fig. 10).

Internally, larger crevasse channel elements possess a tripartite structure (Fig. 11A): the channel proper occupying the middle part is flanked by a levee facies on both sides. The channel proper facies is composed of stacked, small- to medium-scaled trough-cross bedded sandstones (LFT St, Fig. 11C) cutting erosively into the underlying black shales (Fig. 3G). To the top, a succession of LFT Sr, LFT R, and marine black shales (LFT Bm) reflects a fining-upwards. The lithologically more heterogeneous levee facies shows an interfingering of marine black shales and sheet-like non-shale LFT's, such as massive sandstones (Sm), autochthonous root soils (R), and coaly claystones (C), indicating subaerial deposition. In root soils, dm-scale channel elements composed of LFT Sr (Figs. 11A, B, D, F) occur. Crevasse splays are recorded by discrete sheet-like intercalations of the LFT's Sr or Gm being a few decimeters thick and less than 400 m wide (Figs. 11A, G-I; Elliot, 1974). Both the base and top are sharp and even (Fig. 11G), the former being accompanied by abundant reworked *Stigmara* fragments in case of conglomeratic deposits (Figs. 11H and I). Bleaching of black shales can be present down to a depth of a few decimeters beneath crevasse splay and channel sediments (Fig. 11F).

### 4.3. Insect taphonomy

#### 4.3.1. Assemblages composition

Generally, archaeorthopterans (i.e. stem-Orthoptera) dominate all insect assemblages, with ratios ranging from 63 to 74% (Fig. 12A). The assemblages from Phoenix 0 and Peacock 2 are dominated by two species belonging to this group. In contrast, assemblages from Dragon 4 and Phoenix 2 display a more balanced composition, in particular the latter, in which six species each account for ca. 10–13% of the whole assemblage.

#### 4.3.2. Relation of preservation and lithology

Depending on the embedding black shale LFT's, insect assemblages differ considerably in terms of preservation. In the Phoenix 0 assemblage, embedded in LFT Bh, the content of at least partially articulated specimens reaches a value of more than 95% (Fig. 12B). About a third of neopteran individuals display wings in a resting position (Fig. 12C). As for abdomen preservation (Fig. 12D), intact ones predominate (ca. 60%). The loss of abdomen prior to burial represents a minor fraction (20%).

Compared to Phoenix 0, assemblages from LFT  $BL_2$  (Peacock 2, Dragon 4), which are also deeper in the sequence, have fewer wings that are at least partially articulated (70–80% of assemblages; Fig. 12B). Having wings in a resting position is rarely present among the recovered neopterans (Fig. 12C). The type of preservation of the abdomen differs between the two sites (Fig. 12D). However, even though the Peacock 2 assemblage resembles that from Phoenix 0, comparison with that recovered from Dragon 4 is uneasy, as only four specimens for which abdominal preservation can be assessed were recovered from the latter. Indirectly, this suggests that Dragon 4 represents an assemblage of specimens more altered than at Peacock 2.

Finally, the assemblage from Phoenix 2 (LFT  $BL_1$ ), which is the most basally located in the sequence, is dominated by isolated wings (Fig. 12B), in sharp contrast with the three other sites. Among the few neopteran specimens providing information on wing orientation, more than 90% have their wings variously spread (Fig. 12C). As for Dragon 4, because partially articulated (leave alone complete specimens) are extremely rare, abdominal preservation remains an exception, and therefore can barely be evaluated (Fig. 12D).

### 4.4. Relative and absolute data for stratigraphic correlation

#### 4.4.1. Conodonts and goniates

Processing of selected carbonate beds (units 6 and 36 at Peacock Hill; Fig. 10) delivered two dozens of complete and fragmentary conodonts. In general, assemblages are dominated by P1 elements (Figs. 13A–N, S) followed by ramiform elements (Figs. 13O–R, T–V).

However, conodont assemblages differ markedly in their composition, except for *Hindeodella* elements (Figs. 13P–R, T–V) occurring in

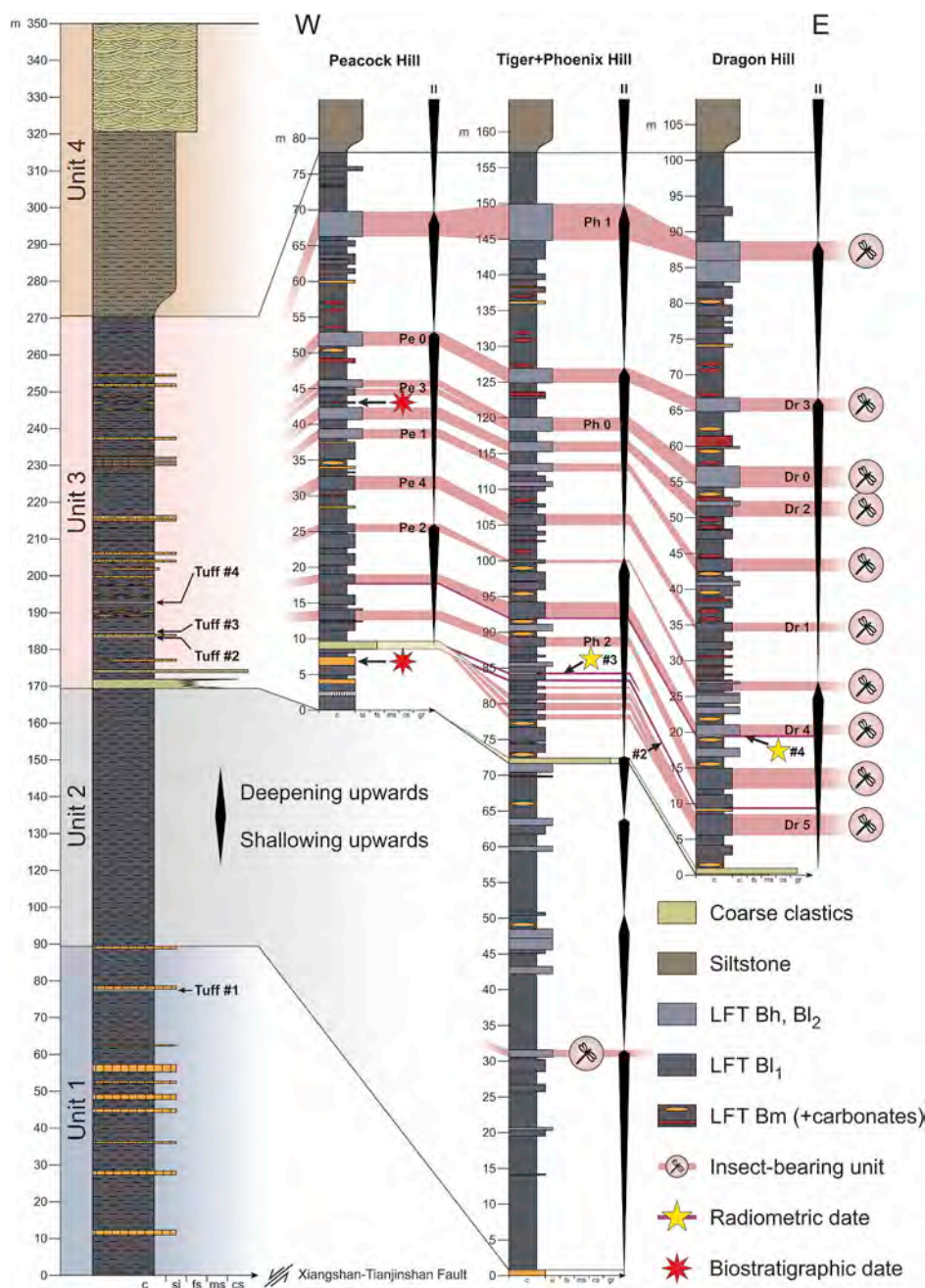


Fig. 8. Profile of the Xiaheyuan section showing 14 insect assemblages gained from ten horizons. Abbreviations: Dr: Dragon. Pe: Peacock. Ph: Phoenix. For detailed legend see Fig. 9.

both limestones. In bed 6 at Peacock Hill, the genus *Declinognathodus* Ellison and Graves, 1941 prevails, and is represented by *Declinognathodus marginodosus* Grayson, 1984 (Figs. 13C, L) and several specimens with unclear species affiliation (Figs. 13A, I, S). Two of the problematic ones (Figs. 13A, S) show similarities with *Declinognathodus lateralis* Higgins and Bouckaert, 1968, as their carina turns towards one parapet without merging with it. In contrast to *D. lateralis*, in which the blade meets the platform in an axial position, the blade-platform junction of the specimens represented in Fig. 13A and 14S is more marginal, causing a bending of the carina. Besides *Declinognathodus*, one element attributable to *Neognathodus* sp. (Fig. 13J) and an M element of *Idioprioniodus conjunctus* Gunnell, 1931 (Fig. 13O) were recovered.

A well-preserved steinkern of *Gastrioceras* cf. *listeri* Sowerby, 1812 (Fig. 14) was found in bed 3 at Dragon Hill, being correlated lithostratigraphically with the conodont-bearing limestone of bed 6 at Peacock Hill. The specimen closely resembles material already published as *Gastrioceras*

*listeri* by Ruan and Zhou (1987) and *Gastrioceras montgomeryense* Miller and Gurley (1896) by Yang (1987) from the Xiaoyuchuan locality in the North Qilian Mountains, 40 km south-east of Xiaheyuan.

The conodont assemblage from bed 36 at Peacock Hill is composed of juvenile and adult *Idiognathodus* specimens (Figs. 13F, G, H, K, M, N and Figs. 13B, D; respectively). Among them, *Idiognathodus praeobliquus* Nemyrovska et al. (1999) (Fig. 13B) was found.

#### 4.4.2. U–Pb dating

Data about tuff lithology and morphology of zircons used for isotope measurements are provided in Supplementary materials 4 and 5; raw data are summarized in Supplementary materials 6 and 7. For tuff #3, an isotopic age of  $314.0 \pm 3.0$  Ma was asserted (MSWD: 2.6; probability of concordance: 0.11; Supplementary material 6). Tuff #4 yielded an age of  $312.0 \pm 3.0$  Ma (MSDW: 3.1, probability of concordance: 0.079; Supplementary material 8).



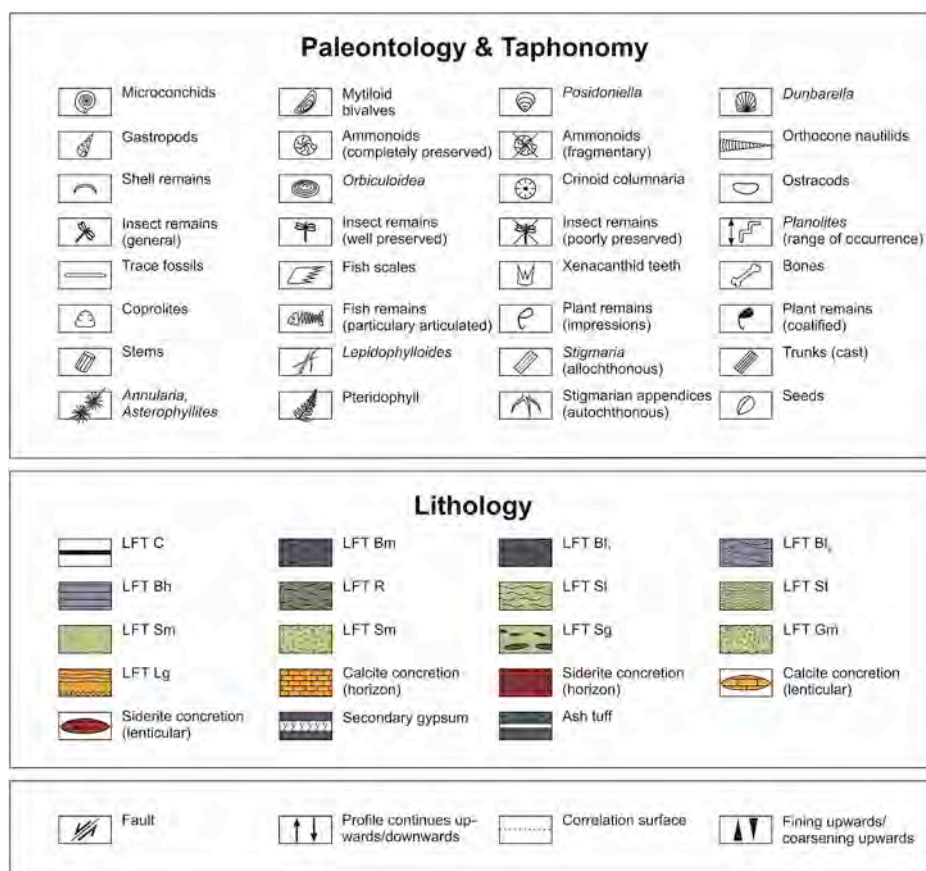


Fig. 9. Legend of signatures used in profiles.

## 5. Discussion

### 5.1. Age and stratigraphy of the Xiaheyan entomofauna

In bed 6, the conodont *Declinognathodus marginodosus* is a cosmopolitan species that defines the homonymous biozone of latest Bashkirian to earliest Moscovian age (Fig. 15; Nemyrovskaya, 1999; Davydov et al., 2010, 2012). This age range for bed 6 can be limited to the latest Bashkirian (Duckmantian), as plesiomorphic features (adcarinal grooves, narrow platform and parapets) of co-occurring *Neognathodus* specimens suggest (Nemyrovskaya, 1999). A latest Bashkirian age is additionally supported by the discovery of a specimen of *Gastrioceras* cf. *listeri* (Fig. 14) in the same bed. *Gastrioceras* species with this conch morphology (coronate shape with angular umbilical margin and coarse ribs) are representatives of the globally applicable late Bashkirian *Branneroceras-Gastrioceras* genus zone (Davydov et al., 2012; Korn and Klug, 2015, Fig. 15). In Western Europe, the FAD of the genus *Gastrioceras* traditionally defines the base of the Westphalian (Korn, 2007).

Concerning bed 36, the conodont species *Idiognathodus praeobliquus* has been reported from the Donets and Midcontinent basins, where it indicates a middle Moscovian (Bolsovian) age (Fig. 15; Nemyrovskaya et al., 1999; Marshall, 2010; Nemyrovskaya, 2017). A post-Bashkirian age for bed 36 is also indicated by juvenile *Idiognathodus* specimens, because their prominent rostral ridges, which reach far beyond the anterior margin of the platform, appear to be too advanced for Bashkirian *Idiognathodus*.

In summary, deposition of the insect-bearing strata started in the latest Bashkirian (Duckmantian) and persisted, at least, into the middle Moscovian (Bolsovian). This biostratigraphic evaluation is consistent with the obtained isotopic ages (Fig. 15), and was already foreshadowed by systematic works on the insect content. Zhang et al.

(2013), for instance, found venation patterns of the Xiaheyan stem-Dictyoptera *Qilianiblatta namurensis* to resemble Westphalian forms. However, given the presence of LFT's B1/2 and Bh in unit 2, including one horizon providing insects (Fig. 8, Supplementary material 3), the insect fossil record could possibly reach back to the middle Bashkirian (Namurian C/Westphalian A). A late Moscovian or even Kasimovian age for the uppermost insect-bearing strata cannot be excluded given the fact that more than 45% of unit 3 is positioned above the uppermost sampled limestone horizon. However, the new age data invalidates a 'Namurian age' and readjusts timelines of Pennsylvanian insect evolution in Eastern Asia.

### 5.2. Depositional environment

Sediments of the Xiaheyan section (units 1–4) recorded the accumulation of a voluminous marine mudstone succession (units 1–3, Fig. 8) that originally possessed a larger thickness, given abundant early diagenetic limestones (Figs. 6B and C). Although radiometric and biostratigraphic data are provided only for the basal part of unit 3 (Fig. 15), it can be concluded that the whole Xiaheyan section (units 1–4) was formed over a period of a few million years. In addition, the depositional system appeared to be prograding, as evidenced by coarsening-upwards cycles of various orders (parasequences in terms of sequence stratigraphy), culminating with fluvial deposits of unit 4 (Figs. 8 and 10). A prograding marine environment prone to a long-time accumulation of thick, partially laminated black shales along with the contemporaneous burial of marine and terrestrial biota is unusual.

At first glance, the aforementioned characteristics are indicative of a prodelta environment. Located at the interface of a river and the ocean, the prodelta is the major sink for the fine-grained suspension load deposited as clay and silt below the storm-wave base. However, two crucial lithological features make this reconstruction questionable.

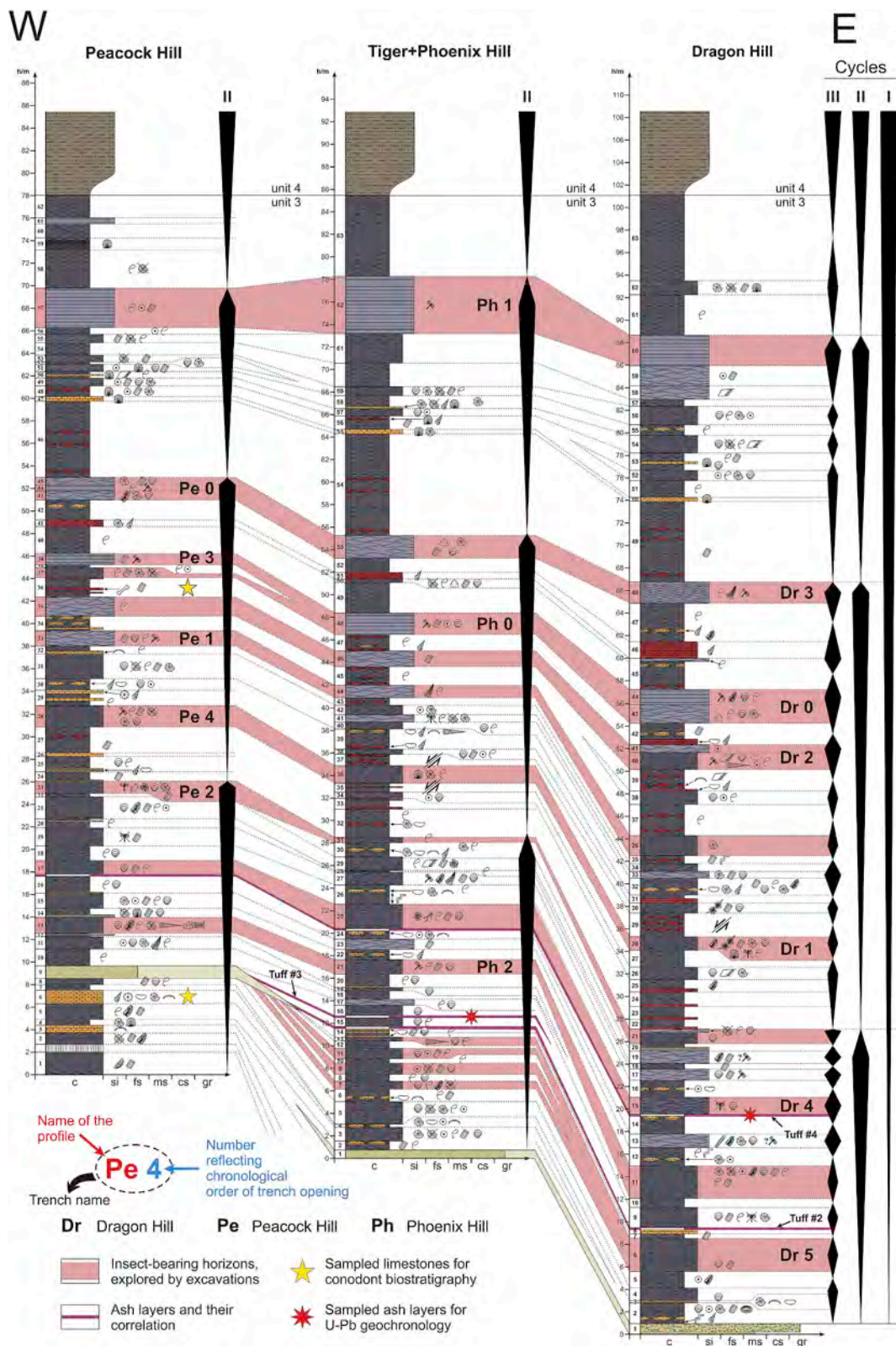
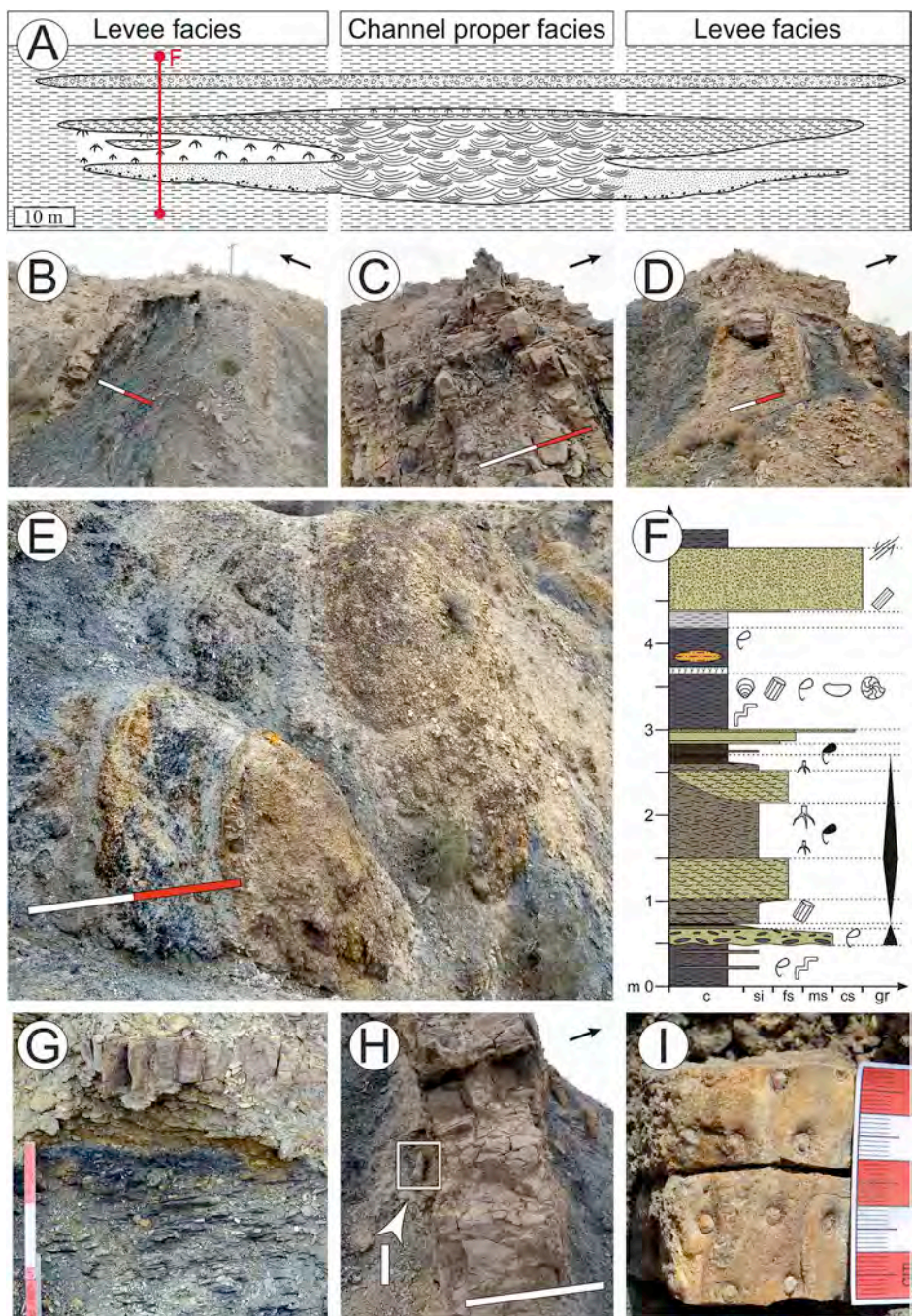


Fig. 10. Detailed profile documentation of unit 3. Note that stratigraphic occurrence of black shale LFT's reflects a cyclic constitution of the section. For legend see Fig. 9.

The first point is the presence of crevasse channel and splay deposits occurring in the basal part of unit 3 (Fig. 8). Since these subaerial to shallow-water sediments interfinger laterally with, and are overlain by black claystones of LFT Bm (Fig. 11A–F), a deep marine (i.e. prodeltaic) formation of the latter is problematic. There are two ways to address

this contradiction: either crevasse deposits represent a sudden phase of sea level drop (lowstand), or black shales were formed, at least partially, at water depths shallower than initially assumed. Under the first option, the stratigraphic level of the crevasse deposits should reflect any shallowing by a change in lithology and/or incisive events (e.g.,





**Fig. 11.** Crevasse channel and splay elements. Black arrows in B, C, D and H point to the top. One section on rule: 1 m. (A) Schematic illustration of lithofacies architecture as shown by the outcrops on Tiger Hill. (B, D) Levee facies. (C) Channel proper facies. (E) Isolated lenticular sandstone element surrounded by black shales. (F) High-resolution profile of the levee facies from A. Note the presence of rooted siltstones and coaly mudstones. For legend see Fig. 9. (G) Sharp, erosional base of the sandstones above black shales of LFT Bm. (H) Conglomerate horizon at Tiger Hill. (I) Allochthonous *Stigmaria* fragment preserved as sandstone cast.

erosion, subaerial exposure) occurring in all sections at Xiaheyan. Lateral correlations, however, demonstrate that crevasse sandstones (e.g., bed 9 at Peacock Hill, Fig. 10) correlate laterally with undisturbed, continuous black shales sequences (e.g., beds 7–17 at Phoenix Hill, Fig. 10). In addition, sandstones occur at different stratigraphic levels, and would therefore require multiple drops in sea level to be explained under this model, which is not supported by lithology. Hence the second option, namely that the enveloping black shales, at least for a part, resulted from deposition at meters to decameters depth, is regarded as more likely.

The deposition of limestone (LFT Lg) is the second characteristic challenging the prodelta model. Based on their internal grading (Fig. 7C)

and the considerable proportion of fragmented bioclasts and peloids in their content (Figs. 7B, D), these rocks must have derived from reworking of carbonates and from their transport as calciturbidites or tempestites. The occurrence of columnal segments of crinoids (and of corals, see Yang, 1992) demonstrates that these limestones deposited under euhaline shallow marine settings, in the photic zone. Prodelta, by contrast, represent turbid environments showing a high siliciclastic input, and receive their sediments essentially from the fluvial system, via suspension fallout and downslope gravitational processes. In other words, a prodelta does not provide conditions suitable for the formation of such carbonates.

A deltaic environment neighboring carbonate settings and into which prodeltaic deposits may prograde was therefore considered. Such



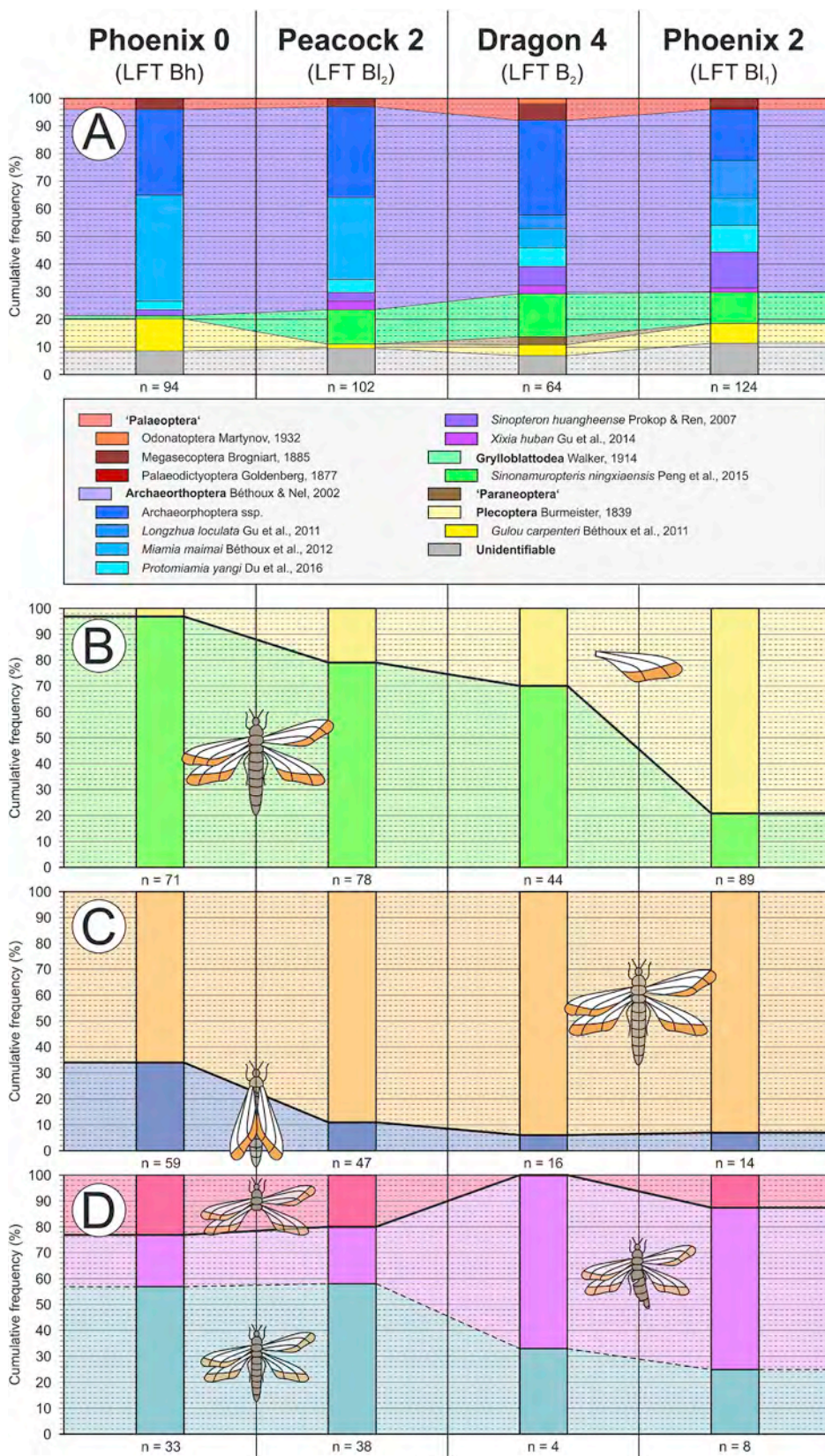


Fig. 12. Insect assemblage composition and preservation in dependence of black shale lithofacies. For stratigraphic position of the selected sites see Fig. 8 (from left to right, excavation sites are ordered from high to low in the sequence). (A) Proportions of taxa. (B) Case of wings recovered with their base, either (green) in connection with thorax or (light yellow) isolated from thorax. (C) Case of neopteran individual recovered with more than one wing and body, wings either (dark blue) in resting position or (orange) not in resting position. (D) Case of individual preserving the posterior part of the thorax, abdomen either (light blue) present and intact, (light pink) or (purple) missing. (For interpretation of the references to color in this figure legend, the reader is referred to the Web version of this article.)

a case is found in interdelta, delta-flank or interdelta lobe systems (Fig. 16), i.e., marine basins or bays that differ from interdistributary bays in their larger size and greater geological longevity (Fisher and McGowen, 1967; Brown, 1969; Baganz et al., 1975). Depending on the relation of subsidence and sediment accumulation rates, such settings

are capable of accumulating considerable amounts of black shales. Lord et al. (2014) found such deposits to reach a thickness of 70 m in the Upper Triassic Hopen Member (De Geerdalen Fm, Svalbard). Additionally, black shales can deposit at shallow depths (meters to decameters) in interdelta bays: depending on the size of the marine basin,



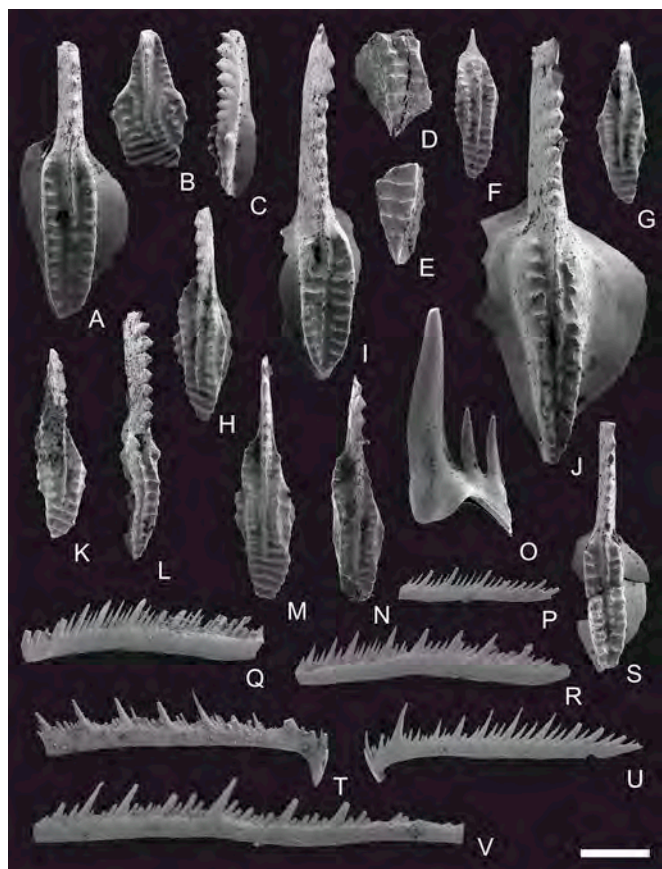


Fig. 13. Conodonts from the insect-bearing part (unit 3). Scale: 200  $\mu\text{m}$ . (A, S) *Declinognathodus* cf. *lateralis* Higgins and Bouckaert, (1968). (B) *Idiognathodus praebliquus* Nemyrovskaya et al. (1999). (C and L) *Declinognathodus marginodosus* Grayson, (1984). (D, E, F, G, H, K, M, N) *Idiognathodus* sp. (I) *Declinognathodus* sp. (J) *Neognathodus* sp. (O) *Idiopriodontus conjunctus* Gunnell, (1931). (M element. P, Q, R, V) *Hindeodella* sp. (T, U) *Hindeodella ibergensis* Bischoff (1957).

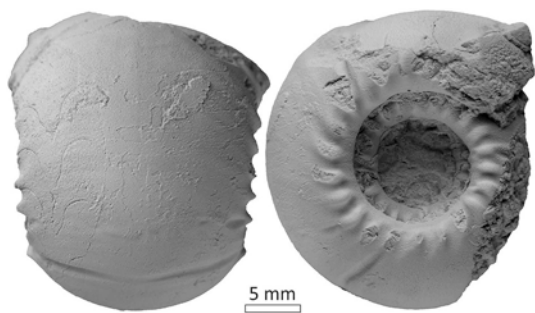


Fig. 14. *Gastrioceras* cf. *listeri* Sowerby, (1812), from bed 3 at Dragon Hill. Ventral and lateral view.

and shape and connection to the open sea, the storm wave base can be found at shallower depths than in the adjacent ocean. If such a situation co-occurs with a stratification of the water column, and a supply with siliciclastic material as in deltaic settings, black shales represent shallow water deposits even above the storm wave base (Hovikoski et al., 2018). The Pennsylvanian Sunbury Shale (Atoka Fm., Arkansas), for instance, is associated with crevasse splay sandstones and thus partially interpreted as interdistributary bay deposit (Balthazor, 1991). Schieber (1998) identified sequence stratigraphic boundaries within the shallow shelf Upper Devonian Chattanooga Shale based on internal erosion surfaces. The ‘interdelta bay’ model is consistent with paleogeographical reconstructions (Fig. 2B) according to which the marine Qilian Basin was framed by deltas.

### 5.3. Formation of laminated black shales

Whereas claystones of LFT Bm represent the common suspension fallout, lenticularly laminated black shale LFT's, by contrast, indicate temporary and spatial interruptions of this background deposition leading to considerable accumulations of biotic remains. Time-averaging is strongly established given considerable compaction (Figs. 4E and F). However, based on their stratigraphic distribution (Fig. 10) and the preservation quality of terrestrial elements (Figs. 12B–D), a relation of laminated black shale lithology and land proximity can be suggested. Accordingly, LFT Bl<sub>1</sub> is most distal, whereas LFT Bl<sub>2</sub> reflects a more proximal position.

Lenticular lamination is a common microfabric known from black shales since the Proterozoic, albeit its formation still remains enigmatic (Schieber et al., 2010). Previous genetic models comprise the accumulation of fecal pellets (Röhl et al., 2001; Schmid-Röhl et al., 2002), dense bioturbation (O'Brien and Slatt, 1990) and the redeposition of mud intraclasts (Schieber et al., 2007). Since lenticularly laminated LFT's at Xiaheyan provide abundant fossils parallel to the bedding plane, any contribution of bioturbation to the black shale fabrics can be discarded. Moreover, keen differences in internal grain size between neighboring mud aggregates (Fig. 4B) contradict an origin from fecal pellets, which are more homogeneous. Differential sagging around shells and quartz grains (Figs. 4D and E), water escape structures and the ellipsoidal three-dimensional geometry of the mud aggregates support a formation of lenticular lamination by the accumulation of water-rich mud aggregates that subsequently faced considerable compaction. In addition, these aggregates were subjected to lateral transport, as evidenced by an increase in sorting and a reduction of mud aggregate size with decreasing land proximity (Fig. 12). Hence, a formation of lenticular lamination by mud redeposition or mud intraclasts, respectively, is then preferred.

As shown experimentally by Schieber et al. (2010), the erosion of muds results in  $\mu\text{m}$ -to mm-sized clasts matching with intraclast sizes observed in LFT's Bl<sub>1/2</sub>. Once eroded, watery mud clasts roll downslope the sea bottom, leading to increased clast roundness and decrease in clast size. According to Schieber et al. (2010) and Plint (2014), mud clast transport is carried out by storm-induced bottom currents, the occurrence of which is supported by (sub-)mm-scale micro-cross stratification and turbidity current intercalations (Schieber and Yawar, 2009, Figs. 4C and D). Given travel velocities in the range of a few centimeters per second, mud redeposition is low-energetic (Schieber et al., 2010). Such a depositional mode minimizes abrasion and disarticulation of simultaneously embedded biota, as documented in the Xiaheyan fossil assemblages.

The strict correlation of fossil occurrence and black shales resulting from redeposition (Fig. 10) indicates a common process of formation. This process caused erosion of muds in shallow waters, and initiated mass mortalities among molluscs of the bay. The latter are represented by non-sorted, low-diverse shell accumulations lacking evidence for transport (Fig. 5B). Deleterious effects were not limited to byssate *Posidoniella*, but also affected vagile-benthic (*Dunbarella*) and nektonic (cephalopods) biota. *Posidoniella* in turn probably possessed a pseudo-planktonic lifestyle, as accumulations on larger plant remains (Fig. 5F) suggest. An epibenthic behavior is unlikely given that suspension-feeding organisms would rapidly sink and suffocate in the soupy water-rich substrate (Nyhuis et al., 2015).

Hence, events forming LFT's Bl<sub>1/2</sub> affected the whole water column. We submit they were storms. Within open bays, the interaction of wave-induced oscillation, Coriolis deflection, and shoreline dissipation provokes ground-touching currents capable of eroding muds and redeposit them basinwards (Plint, 2014; Hovikoski et al., 2018). Reworking and resuspension of oxygen-deficient muds is known to trigger mass mortality among gill-breathing suspension feeders (Westermann, 1996; Ellis et al., 2002). Although molluscs have adaptations to cope with rising anoxia and turbidity, respiration can be blocked above a certain

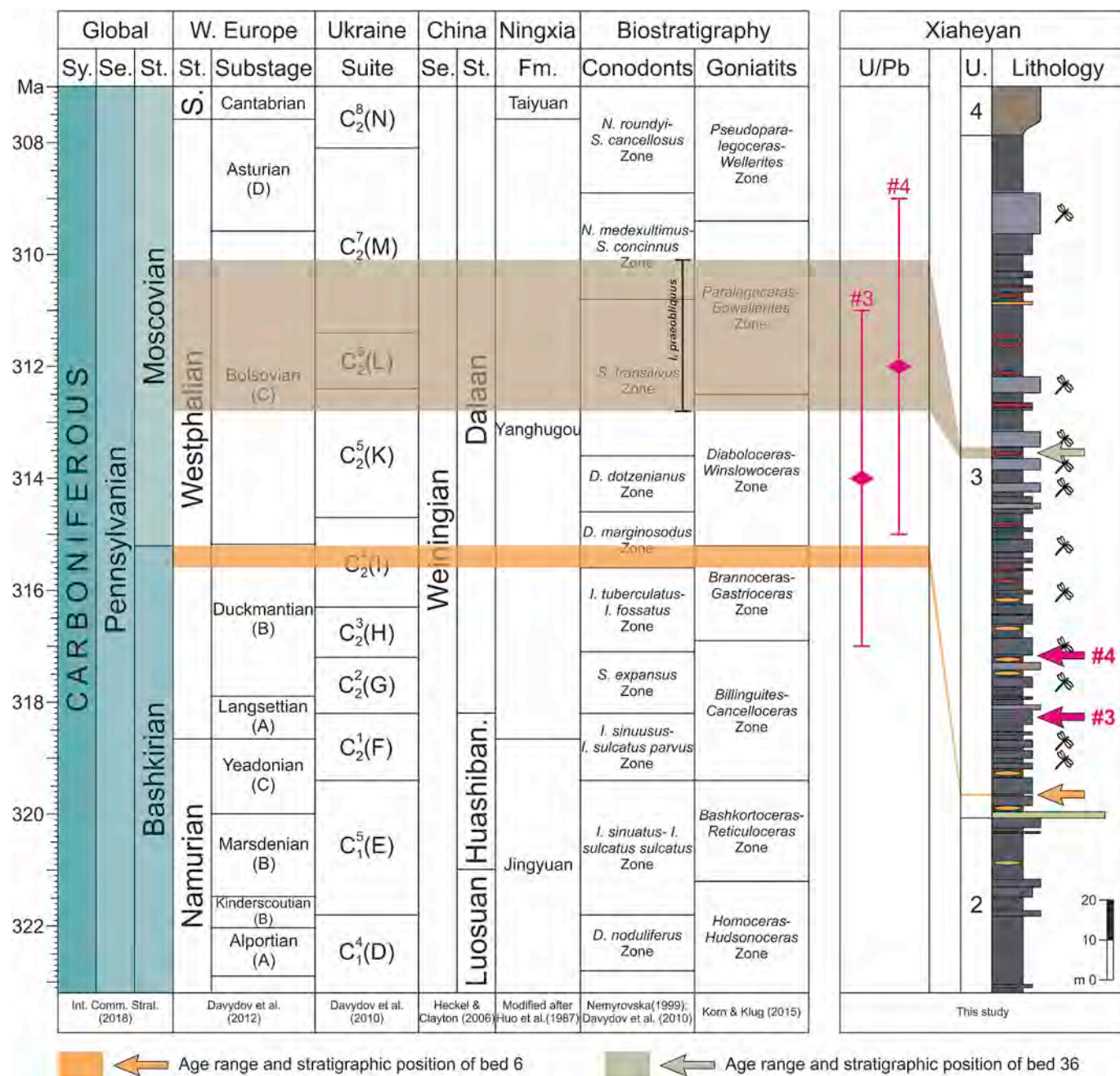


Fig. 15. Age and stratigraphic correlation of unit 3. Formation of insect fossiliferous beds reached from the latest Bashkirian at least into the middle Moscovian.

threshold leading to asphyxia (Peterson, 1985; Bricelji et al., 1984; Ward and MacDonald, 1996; Thrush et al., 2004).

Based on the dominance of dm-sized plant remains and complete insects among their fossil assemblages (Fig. 12B), as well as their stratigraphic position at the top of the shallowing-up parasequences (Figs. 8 and 10), LFT Bh shales were formed in a proximal position to the delta (Fig. 16E). Horizontal lamination and the lack of sand-sized quartz grains point to suspension fallout in a non-turbulent water body. The low abundance of fossils (especially marine groups) may result from a broad range of reasons, such as enhanced sedimentation rate and/or low salinity.

#### 5.4. Factors controlling insect input and preservation

First of all, sediment anoxia and negligible bioturbation were crucial preconditions for insect fossilization, and occurred in all LFT's. Hence,

we consider pre- and syn-depositional circumstances as forces controlling insect occurrence and preservation. In LFT Bm, the lack of insects probably resulted from low sedimentation rates that favored decomposition and scavenging (Fig. 16B). This assessment is supported by rare, highly macerated plant remains and fish fossils. In LFT's Bl<sub>1/2</sub>, insects were rapidly buried by current-driven mud intraclast flows (Figs. 16C and D), as suggested by the considerable proportions of damaged and incomplete specimens, and of twisted wings.

The relation of preservation and black shale lithology among all insect groups (Figs. 12 B–D) can be explained predominantly by transport distance (and, accordingly, floating time and resulting decay). Hence, insect completeness was a function of land proximity, with decreasing preservation quality resulting from increasing distance from land. The taxonomically balanced assemblage of LFT Bl<sub>1</sub> (Phoenix 2; Fig. 12A) suggests that it is a mixture of several local communities, i.e., an allochthonous assemblage. This proposal is corroborated by a



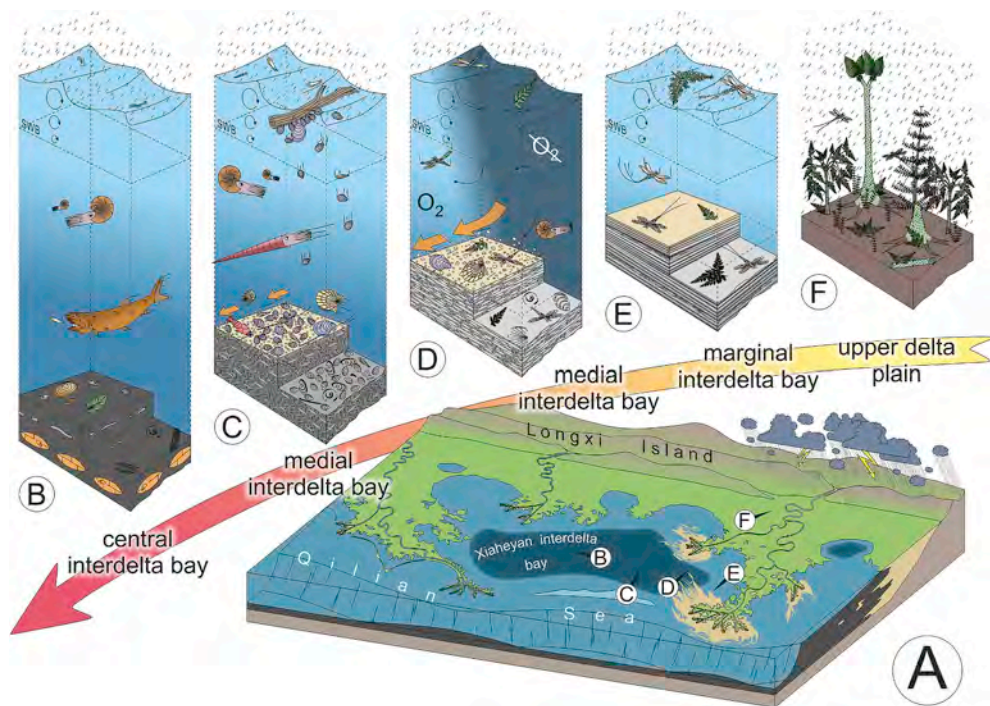


**Fig. 16.** Depositional environment of the Xiaheyuan section. (A) Interdelta bay including the positions of B to F. (B) Formation of LFT Bm at low rates of deposition. (C) Formation of LFT Bl<sub>1</sub> in settings distant to the delta. (D) Formation of LFT Bl<sub>2</sub> in settings medial to the delta. (E) Formation of LFT Bh in settings proximal to the delta. (F) Upper delta plain forests as hypothetical habitat of the insects.

generally poor preservation, indicative of advanced decay and floating time, itself assumed to reflect a setting distant from land. In contrast, the taxonomically depauperate assemblage recovered from LFT Bh (Phoenix 0) is then regarded as a more local community. Accordingly, insect preservation is dominated by pristine specimens. Finally, assemblages recovered from LFT Bl<sub>2</sub> (Peacock 2 and Dragon 4) display characteristics intermediate between the two others. Taxonomic composition at Peacock 2, more unbalanced than at Dragon 4, suggests that it is the most proximal of the two. The observed sequence is consistent with the location of these sites along the stratigraphic sequence (Fig. 10).

In order to make this proposal more tangible we provide a tentative model of insect deposition (Fig. 17). It assumes a wind-induced initial input (Fig. 17A), since arthropods supposed to be ground- or litter-dwelling (as opposed to plant-dwelling arthropods and effective insect fliers), such as myriapods and stem-Dictyoptera, are very rare or absent in Xiaheyuan assemblages. Insects stuck on water surface are then cast away by surface fluvial and then oceanic currents, ultimately provoking their death by exhaustion. Decay progresses while insect carcasses are further dragged seawards. Carcasses sink once disarticulation is sufficiently advanced. According to this model disarticulated insect remains predominantly accumulate in settings distal to land. In other words, it does not account for the occurrence of pristine insect remains in areas closer to land.

This, in turn, can be explained by 'sinking agents', i.e. events inducing insect carcasses to overcome surface tension before they incur advanced decay. Rainfall, waves and wind can act as such agents. Neck (1992), for instance, reported a high proportion of insects in the pleuston of the Cox Bay (Texas Gulf Coast) in the aftermath of a heavy precipitation event. Martínez-Delclòs and Martinell (1993) reported that no insects were left on water surface after a day of rainfall and/or wind. Finally, Peck (1994) observed an elevated input of insects into the seaways between the Galápagos Islands during the 1992 El Niño climatic event. In summary, a storm event would compose an efficient sinking agent.

Then, assuming a distribution of insects at the water surface as in Fig. 17A, with 5 distinct carcasses (Fig. 17B), rainfall, wind and/or waves induce sinking of the floating ones (Fig. 17C). In the interdelta bay setting, after reaching the seafloor, insect carcasses might have been further altered by storm-induced bottom currents carrying mud

intraclasts (Fig. 17D). Concurrently, this would have contributed their entombment. In areas closer to land or to the delta (LFT Bh), increased sedimentation rates due to suspension fallout might have resulted into fast burial of insect carcasses. This model accounts for the observed correlation between lithology and insect preservation (Fig. 12).

##### 5.5. Xiaheyuan and Hagen-Vorhalle: similar deltaic insect taphotypes?

Fossil insects from Hagen-Vorhalle (Germany) represent the earliest diverse entomofauna worldwide, dated from the earliest Bashkirian (late Marsdenian; Ilger, 2011). Insects occur in siltstones (Schöllmann, 1999) resembling LFT Bh in terms of shale fabric and abundance of complete specimens. These horizons are part of a succession that shares a similar lithology with the Xiaheyuan section but represents another deltaic sub-environment. The high proportion of crevasse deposits and frequent freshwater and terrestrial elements among the Hagen-Vorhalle assemblages (bivalves, eurypterids, arachnids, myriapods, xenacanthids, amphibians and dm- to m-sized plant remains) reflect deposition in an interdistributary bay (Huwe, 2006, Fig. 16). However, both localities diverge in insect preservation, indicating distinct taphonomic pathways within fluvially-dominated deltas.

First, the Hagen-Vorhalle entomofauna possesses a higher proportion of complete insects (Brauckmann and Schöllmann, 2005). This difference probably mirrors greater delta proximity of the Hagen-Vorhalle setting. Second, the comparatively higher abundance of terrestrial ground-dwelling arthropods indicates rivers as important insect suppliers at Hagen-Vorhalle. This assessment is additionally supported by the occurrence of insect nymphs (Brauckmann and Schöllmann, 2005). As a third point, the Hagen-Vorhalle entomofauna lacks the preservation of anatomical microstructures, e.g., body setation, which have been identified in megasecopteran insects from Xiaheyuan (Prokop et al., 2016). This difference might be connected to taphonomic biases at Hagen-Vorhalle as this site faced considerable thermal and tectonic overprints connected to the Variscan Orogeny. Brauckmann et al. (1985) for instance found structural details of insects and arachnids from Hagen-Vorhalle to be commonly tectonically obliterated.

Based on black shales lacking bioturbation and biofacies, Ilger (2011) reconstructed anoxic, euhaline bottom waters, and oxygenated oligohaline shallow waters at Hagen-Vorhalle. A well-developed water

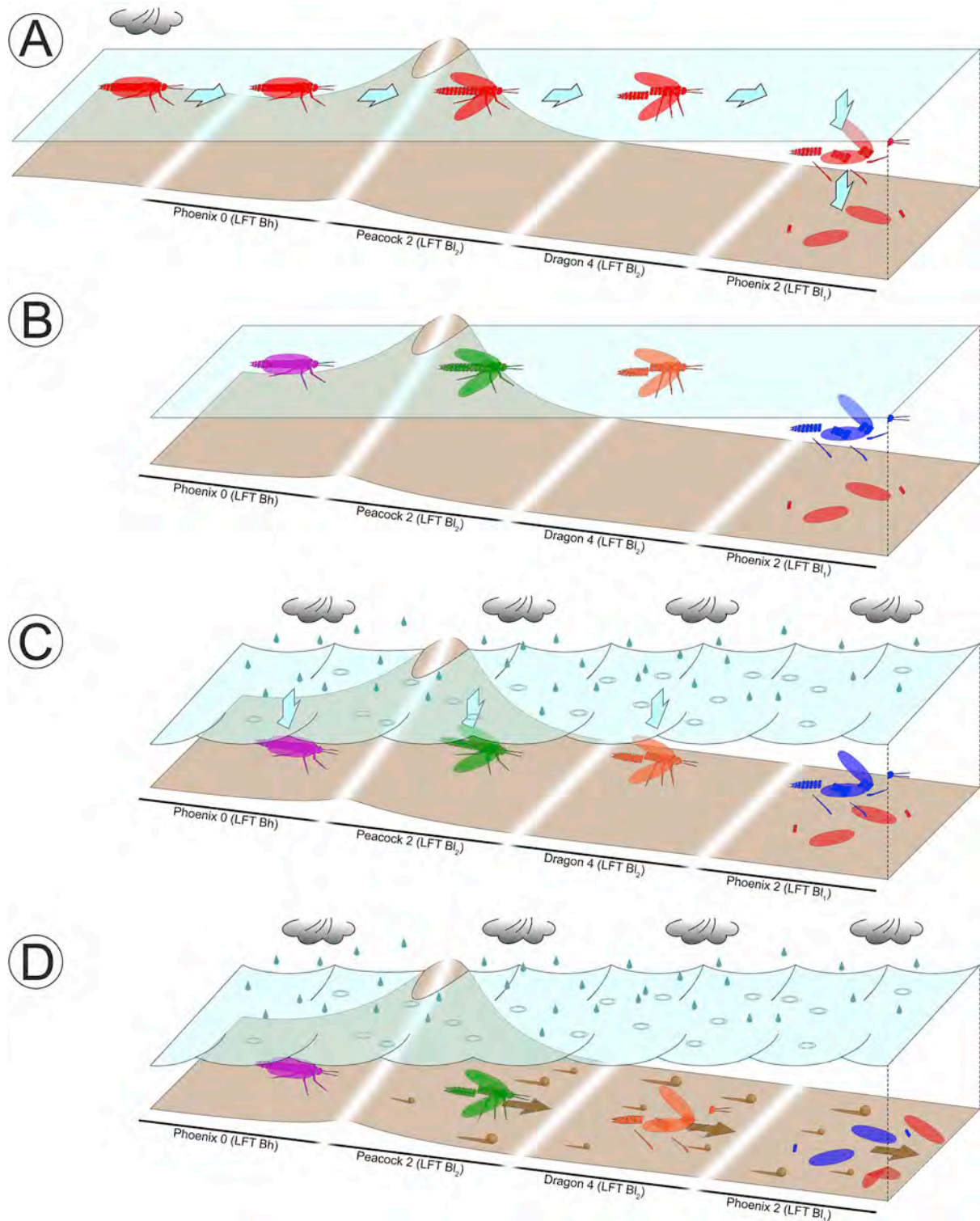


**Fig. 17.** Insect taphonomic model. (A) Preservation as a function of floating time. Note decreasing preservation quality with increasing distance from land due to decay. (B–C) Proposed taphonomic model and resulting assemblages. (B) After having been blown onto the water surface by winds, insects disperse across the interdelta environment as in (A). (C) Sinking initiated by rainfall, wind and/or wave during storms. (D) In the interdelta bay, subsequent storms provoke mud erosion in shallow waters and trigger downslope sediment flows that rework, twist and bury specimens below the storm-wave base.

stratification of the water body at Hagen-Vorhalle, and its absence at Xiaheyan, might be connected to the localities' positions relative to the delta. As documented in the recent Mississippi delta, enclosed water bodies possess stratification if they are prone to persistent freshwater inflow and low tidal range (Georgiou and McCorquodale, 2002). In the larger Xiaheyan interdelta bay, freshwater overflow was possibly

quickly dispersed by currents and waves (Rong et al., 2014). Low surface salinity at Hagen-Vorhalle could explain why non-marine pseudoplanktonic *Naiadites* claimed the paleoecological niche that was likely filled by marine *Posidoniella* at Xiaheyan (see Huwe, 2006).

In summary, we conclude that Hagen-Vorhalle and Xiaheyan represent distinct deltaic taphotypes. Both localities, and other insect



occurrences found in coastal settings (Brauckmann, 1982; Schultze et al., 1993; Ponomareva et al., 1998; Beckemeyer and Hall, 2007; Schneider et al., 2016) highlight the importance of fossiliferous marginal marine settings in deciphering insect evolution during the Palaeozoic.

## 6. Conclusions

- (1) The Xiaheyuan section displays a regressional marine succession starting with an open bay and culminating in the lower coastal plain.
- (2) Insect-bearing strata form part of interdelta bay deposits that are assigned to the Yanghugou Fm. Multiple proxies indicate that deposition started in the latest Bashkirian (late Duckmantian) and persisted at least until the middle Moscovian (Bolsvian).
- (3) Deltaic environments possess highly variable insect taphonomic pathways. Composition and preservation of insect taphocoenoses formed in interdelta bays are controlled by an initial wind-driven insect recruitment, disarticulation during floating, the recurrence of sinking events, and compactional time-averaging. Lithology and insect taphocoenoses abundance skewness and preservation quality correlate with proximity to land.
- (4) Entombment of insect carcasses in laminated black shales results from either suspension fallout in settings proximal to land, or, in more distal areas, storm-induced bottom currents carrying mud intraclasts.

## Declaration of competing interest

The authors declare that the research was conducted in the absence of any commercial or financial relationships that could be construed as a potential conflict of interest.

## Acknowledgements

We gratefully thank Yingying Cui (Guangzhou), Yingnan Li, Lei Li, Zhipeng Zhao, Bingyue Zheng (all Beijing) and the motivated biology students of the Capital Normal University for their encouraging support in organizing and realizing the field works. Michael Amler (Cologne), Jim Barrick (Austin), Stephen J. Godfrey (Solomons), Keyi Hu (Nanjing), Christina Ifrim (Heidelberg), Ronny Rößler (Chemnitz) and Jens Zimmermann (Neubrandenburg) are acknowledged for their efforts on identification of conodonts, molluscs and plants. Olaf Elicki (Freiberg), Zhuo Feng (Kunming), Birgit Gaitzsch (Freiberg), Robert A. Gastaldo (Waterville), Ludwig Luthardt (Chemnitz), Giliane Odin (Cork), Lothar Schöllmann (Münster) and Jens Zimmermann (Neubrandenburg) contributed to discussions of sediment diagenesis, depositional environment and stratigraphy. Gitta Schneider and Delia Rösel (both Freiberg) supported the work with helpful hints for rock processing and U/Pb dating. Ai Lun (Freiberg) helped in translating Chinese literature. JWS acknowledges the support of his work by the grants of the German Research Foundation DFG SCHN408/22-1 and the Russian Government Program of Competitive Growth of Kazan Federal University. This research was supported by the National Natural Science Foundation of China (No. 31730087, 41688103), the Program for Changjiang Scholars and Innovative Research Team in University (IRT-17R75) and Project of High-level Teachers in Beijing Municipal Universities (No. IDHT20180518). Careful reviews by three anonymous reviewers improved the content and clarity of the manuscript.

## Appendix A. Supplementary data

Supplementary data to this article can be found online at <https://doi.org/10.1016/j.palaeo.2019.109444>.

## References

- Baganz, B.P., Horne, J.C., Fenn, J.C., 1975. Carboniferous and recent Mississippi lower delta plains: a comparison. *Trans. Gulf Coast Assoc. Geol. Soc.* 25, 183–191.
- Balthazor, D.A., 1991. *Sedimentology of the Bedford-Berea Sequence (Early Mississippian)*, Williams Field. Western Michigan University, Master's Thesis, Michigan, pp. 946.
- Beckemeyer, R.J., Hall, J.D., 2007. The entomofauna of the Lower Permian fossil insect beds of Kansas and Oklahoma, USA. *Afr. Invertebr.* 48, 23–39.
- Béthoux, O., Cui, Y., Kondratieff, B., Ren, D., 2011. At last, a Pennsylvanian stem-stonefly (Plecoptera) discovered. *BMC Evol. Biol.* 11, 248. <https://doi.org/10.1186/1471-2148-11-248>.
- Béthoux, O., Gu, J.-J., Ren, D., 2012a. A new upper carboniferous stem-orthopteran (insecta) from Ningxia (China). *Insect Sci.* 19, 153–158. <https://doi.org/10.1111/j.1744-7917.2011.01468.x>.
- Béthoux, O., Gu, J.-J., Yue, Y., Ren, D., 2012b. *Miamia maimai* n. sp., a new Pennsylvanian stem-orthopteran insect, and a case study on the application of cladotypic nomenclature. *Foss. Rec.* 15, 103–113. <https://doi.org/10.1002/mmg.201200008>.
- Bischoff, G., 1957. Die Conodonten-Stratigraphie des rheinherzynischen Unterkarbons mit Berücksichtigung der Wocklumeria-Stufe und der Devon-Karbon-Grenze. *Abh. Hess. L.-A. Bodenforsch.* 19, 1–64.
- Brauckmann, C., 1982. Der Schwertschwanz *Euproops* (Xiphosurida, Limulina, Euproopacea) aus dem Ober-Karbon des Piesbergs bei Osnabrück. *Osnabrücker Naturwiss. Mittl.* 16, 27–30.
- Brauckmann, C., Koch, L., Kemper, M., 1985. Spinnentiere (Arachnida) und Insekten aus den Vorhalle-Schichten (Namurium B; Ober-Karbon) von Hagen-Vorhalle (West-Deutschland). *Geol. Palaontol. Westfalen* 3, 5–131.
- Brauckmann, C., Schneider, J.W., 1996. Ein unterkarbonisches Insekt aus dem Raum Bitterfeld/Delitzsch (Pterygota, Arnsbergium, Deutschland). *Neues Jahrb. Geol. Pal.* 1, 17–30.
- Brauckmann, C., Schöllmann, L., 2005. Insecta (insekten). In: Hendricks, A. (Ed.), *Als Hagen am Äquator lag. Die Fossilien der Ziegeleigrube Hagen-Vorhalle. Landschaftsverband Westfalen-Lippe, Münster*, pp. 8–125.
- Brauckmann, C., Schöllmann, L., Sippel, W., 2003. Die fossilen Insekten, Spinnentiere und Eurypteriden von Hagen-Vorhalle. *Geol. Palaontol. Westfalen* 59, 1–89.
- Bricelj, V.M., Malouf, R.E., de Quillfeldt, C., 1984. Growth of juvenile *Mercenaria mercenaria* and the effect of resuspended bottom sediments. *Mar. Biol.* 84, 167–173.
- Brongniart, A.T., 1828. *Prodrome d'une histoire des végétaux fossils*. l'imprimerie de F.G. Levrault, Strasbourg, pp. 198.
- Brongniart, C., 1893. *Recherches pour servir à l'histoire des insectes fossiles des temps primaires précédées d'une étude sur la nervation des ailes des insectes*. *Bull. Soc. Ind. Minér. Saint-Etienne* 3, 124–615.
- Brown, L.F., 1969. Virgil and Lower Wolfcamp repetitive environments and the depositional model in north-central Texas. In: Elam, J.C., J.C., Chuber, S., S. (Eds.), *Cyclic Sedimentation in the Permian Basin: Midland, Texas*, vol. 56. *West Texas Geol. Soc. Pub.*, pp. 115–134.
- Carpenter, F.M., 1997. Insecta. In: Shabica, C.W., Hay, A.A. (Eds.), *Richardson's Guide to the Fossil Fauna of Mazon Creek*. Northeastern Illinois University, Chicago 184–193.
- Cope, T., Ritts, B.D., Darby, B.J., Fildani, A., Graham, S.A., 2005. Late Paleozoic sedimentation on the northern margin of the North China block: implications for regional tectonics and climate change. *Int. Geol. Rev.* 47 <https://doi.org/10.2747/0020-6814.47.3.27010.2747/0020-6814.47.3.270>. 270–269.
- Cui, Y., Béthoux, O., Ren, D., 2011. Intraindividual variability in *Sinonamuropteridae* forewing venation (Grylloblattida; Late Carboniferous): taxonomic and nomenclatural implications. *Syst. Entomol.* 36, 44–56. <https://doi.org/10.1111/j.1365-3113.2010.00545.x>.
- Davydov, V.I., Crowder, J.L., Schmitz, M.D., 2010. High-precision U-Pb zircon age calibration of the global Carboniferous time scale and Milankovitch band cyclicity in the Donets Basin, eastern Ukraine. *Geochem. Geophys. Geosyst.* 11, Q0AA04. <https://doi.org/10.1029/2009GC002736>.
- Davydov, V.I., Korn, D., Schmitz, M.D., 2012. The carboniferous period. In: Gradstein, F.M., Ogg, J.G., Schmitz, M.D., Ogg, G.M. (Eds.), *The Geologic Time Scale 2012*. Elsevier and Science Press, Oxford, pp. 603–651. <https://doi.org/10.1016/B978-0-444-59425-9.00023-8>.
- de Koninck, L.G., 1885. *Faune du calcaire Carbonifère de la Belgique*. 5. Lamellibranches. *Ann. Mus. Roy. Hist. nat. Bel.* 11, 1–283.
- d'Orbigny, A., 1847. *Considérations zoologiques et géologiques sur les Brachiopodes ou Palliobranches*. *Comptes Rendus Hebd. Seances Acad. Sci.* 25, 193–195.
- Du, S., Béthoux, O., Gu, J., Ren, D., 2016. *Protomiaia yangi* gen. et sp. nov. (Early Pennsylvanian; Xiaheyuan, China), a sexually dimorphic Palaeozoic stem-Orthoptera. *J. Syst. Palaeontol.* 15, 193–204. <https://doi.org/10.1080/14772019.2016.1154899>.
- Dunlop, J., 2010. Geological history and phylogeny of Chelicerata. *Arthropod Struct. Dev.* 39, 124–142. <https://doi.org/10.1016/j.jasid.2010.01.003>.
- Elliott, T., 1974. Interdistributary bay sequences and their genesis. *Sedimentology* 21, 611–622. <https://doi.org/10.1111/j.1365-3091.1974.tb01793.x>.
- Ellis, J., Cummings, V., Hewitt, J., Thrush, S., Norkko, A., 2002. Determining effects of suspended sediment on condition of a suspension feeding bivalve (*Atrina zelandica*): results of a survey, a laboratory experiment and a field transplant experiment. *J. Exp. Mar. Biol. Ecol.* 267, 147–174. [https://doi.org/10.1016/S0022-0981\(01\)00355-0](https://doi.org/10.1016/S0022-0981(01)00355-0).
- Ellison, S., Graves, R.W., 1941. Lower Pennsylvanian (Dimple Limestone) Conodonts of the Marathon Region. vol. 14. *Missouri University, School of Mines and Metallurgy, Bulletin, Texas*, pp. 1–13.
- Fisher, W.L., McGowen, J.H., 1967. Depositional systems in the Wilcox Group of Texas and their relationship to occurrence of oil and gas. *Trans. Gulf Coast Assoc. Geol. Soc.* 17, 105–125.

- Georgiou, I., McCorquodale, J.A., 2002. Stratification and circulation in lake Pontchartrain. In: Spaulding, M.L. (Ed.), *Estuarine and Coastal Modeling. Proceedings of the Seventh International Conference*. American Society of Civil Engineers, Reston, pp. 140–151.
- Grayson, R.C., 1984. Morrowan and Atokan (Pennsylvanian) conodonts from the Northwestern margin of the Ac buckle Mountains southern Oklahoma. *Okla. Geol. Surv. Bull.* 136, 41–63.
- Gu, J.-J., Béthoux, O., Ren, D., 2011. *Longzhua loculata* n. gen. n. sp., one of the most completely documented Pennsylvanian Archaeorthoptera (Insecta; Ningxia, China). *J. Paleontol.* 85, 303–314. <https://doi.org/10.1666/10-085.1>.
- Gunnell, F.N., 1931. Conodonts from the fort Scott limestone of Missouri. *J. Paleontol.* 26, 244–252.
- Higgins, A.C., Bouckaert, J., 1968. Conodont stratigraphy and paleontology of the Namurian of Belgium. *Mém. Explic. Cart. Géol. Min. Bel.* 10, 1–64.
- Hong, Y., Peng, D., 1995. Namurian insects of Qilianshan Mt. W. China. *Collection Pacific Science Congress (Beijing, 1995, vol. 134 Scientific Program Committee*.
- Hovikoski, J., Lemiski, R., Gingras, M., Pemberton, G., MacEarchern, J.A., 2018. Ichnology and sedimentology of a mud-dominated deltaic coast: upper cretaceous Alderson member (Lea Park Fm), west. *Can. J. Sediment. Res.* 78, 803–824. <https://doi.org/10.2110/jsr.2008.089>.
- Huwe, S.I., 2006. Die Bivalvenfauna aus dem Namurium B (Pennsylvanium) von Hagen-Vorhalle – taxonomie, Faunenbeziehungen und Paläoökologie. *Geol. Paläontol.* 40, 63–171.
- Ilger, J.-M., 2011. Young bivalves on insect wings: a new taphonomic model of the Konservat-Lagerstätte Hagen-Vorhalle (early Late Carboniferous; Germany). *Palaeogeogr. Palaeoclimatol. Palaeoecol.* 310, 315–323. <https://doi.org/10.1016/j.palaeo.2011.07.023>.
- Korn, D., 2007. Goniatiten von der Namur/Westfal-Grenze im Rheinischen Schiefergebirge (Cephalopoda, Ammonoidea; Oberkarbon; Deutschland). *Geol. Palaontol. Westfalen* 69, 5–45.
- Korn, D., Klug, C., 2015. Paleozoic ammonoid biostratigraphy. In: Klug, C., Korn, D., De Baets, K., Kruta, I., Mapes, R.H. (Eds.), *Ammonoid Paleobiology: from Macroevolution to Palaeogeography*. Springer, Dordrecht, pp. 299–328. [https://doi.org/10.1007/978-94-017-9633-0\\_12](https://doi.org/10.1007/978-94-017-9633-0_12).
- Li, Y., Béthoux, O., Pang, H., Ren, D., 2013a. Early Pennsylvanian Odonatoptera from the Xiaheyuan locality (Ningxia, China): new material, taxa, and perspectives. *Foss. Rec.* 16, 117–139. <https://doi.org/10.1002/mmg.201300006>. + 244 (corrigendum).
- Li, Y., Ren, D., Pecharová, M., Prokop, J., 2013b. A new palaeodictyopterid (Insecta: Palaeodictyoptera: Spilapteridae) from the Upper Carboniferous of China supports a close relationship between insect faunas of Qilianshan [sic] (northern China) and Laurussia. *Alcheringa* 37, 487–495.
- Liu, G., 1990. Permo-Carboniferous paleogeography and coal accumulation and their tectonic control in the North and South China continental plates. *Int. J. Coal Geol.* 16, 73–117. [https://doi.org/10.1016/0166-5162\(90\)90014-4](https://doi.org/10.1016/0166-5162(90)90014-4).
- Liu, Z., Cui, H., Xu, S., Wu, P., Zhang, H., Zhang, W., Feng, H., Li, L., Li, J., Xu, Q., Li, M., 2014. Sedimentary systems in maximum flooding period of Carboniferous in Zhongwei area and adjacent regions. *Mar. Geol. Front.* 30, 1–10.
- Lord, G.S., Solvi, K.H., Ask, M., Mork, A., Hounslow, M.W., Paterson, N.W., 2014. The Hopen member: a new member of the triassic de Geerdalen formation. *Svalbard. Nor. Petrol. Direct. Bull.* 11, 81–96.
- Lu, L., Fang, X., Ji, S., Pang, Q., 2002. A contribution to the knowledge of the Namurian in Ningxia. *Acta Geosci. Sin.* 23, 165–168.
- Marshall, T.R., 2010. Conodont-based Correlation of Major Cyclothem in Lower Cherokee Group (Lower Desmoinesian, Middle Pennsylvanian). Oklahoma to Iowa. Ph.D. thesis, University of Iowa, Iowa City, pp. 248.
- Martínez-Delclòs, X., Martinell, J., 1993. Insect taphonomy experiments. Their application to the Cretaceous outcrops of lithographic limestones from Spain. *Kaupia Darmstadter Beiträge zur Naturgeschichte* 2, 133–144.
- McCoy, F., 1851. A Synopsis of the Classification of the British Palaeozoic Rocks, with a Systematic Description of the British Palaeozoic Fossils. Parker & Son, London, pp. 116.
- Meek, F.B., 1874. New genus *Euchondria* Meek. *Am. J. Sci.* 3, 445.
- Miall, A., 1996. *The Geology of Fluvial Deposits, Sedimentary Facies, Basin Analysis and Petroleum Geology*. Springer, Berlin, Heidelberg, pp. 582.
- Miller, S.A., Gurley, W.F.E., 1896. New species of Paleozoic invertebrates from Illinois and other states. *Illinois State Mus. Nat. Hist. Bull.* 11, 1–50.
- Neck, R.W., 1992. Fluvial transport of terrestrial and aquatic insects into an estuary along the central Texas coast. *Tex. J. Sci.* 44, 429–435.
- Nemyrovskaya, T.I., 1999. Bashkirian conodonts of the Donets basin, Ukraine. *Ser. Geol.* 119, 1–115.
- Nemyrovskaya, T.I., 2017. Late Mississippian – middle Pennsylvanian conodont zonation of Ukraine. *Stratigraphy* 14, 299–318. <https://doi.org/10.29041/strat.14.1-4>. 299–318.
- Nemyrovskaya, T.I., Perret-Mirouse, M.-F., Alekseev, A., 1999. On Moscovian (late carboniferous) conodonts of the Donets basin, Ukraine. *Neues Jahrb. Geol. Paläontol. Abh.* 214, 169–194. <https://doi.org/10.1127/njgpa/214/1999/169>.
- Newell, N.D., 1938. Late paleozoic pelecypods: Pectinacea. *State Geol. Surv. Kansas* 10, 1–123.
- Nicholson, H.A., 1873. Contributions to the study of the errant annelids of the older Paleozoic rocks. *Proc. R. Soc. Lond.* 21, 288–290.
- Nie, S., 1991. Paleoclimatic and paleomagnetic constraints on the Paleozoic reconstructions of south China, North China and Tarim. *Tectonophysics* 196, 279–308. [https://doi.org/10.1016/0040-1951\(91\)90327-0](https://doi.org/10.1016/0040-1951(91)90327-0).
- Nyhuis, C.J., Amler, M.R.W., Herbig, H.-G., 2015. Facies and palaeoecology of the late Viséan *Actinopteria* black shale event in the Rhenish Mountains (Germany, Mississippian). *Z. Dtsch. Ges. Geowiss.* 166, 55–69.
- O'Brian, N.R., Slatt, R.M., 1990. *Argillaceous Rock Atlas*. Springer, New York City, pp. 141.
- Odin, G.P., Rouchon, V., Béthoux, O., Dong, R., 2018. Gypsum growth induced by pyrite oxidation jeopardises the conservation of fossil specimens: an example from the Xiaheyuan entomofauna (Late Carboniferous, China). *Palaeogeogr. Palaeoclimatol. Palaeoecol.* 507, 15–29. <https://doi.org/10.1016/j.palaeo.2018.05.035>.
- Pecharová, M., Ren, D., Prokop, J., 2015. A new palaeodictyopteroid (Megasecoptera: Brodiopterae) from the Early Pennsylvanian of northern China reveals unique morphological traits and intra-specific variability. *Alcheringa* 39, 236–249. <https://doi.org/10.1080/03115518.2015.993299>.
- Peck, S.B., 1994. Sea-surface (pleuston) of insects between islands in the Galápagos Archipelago, Ecuador. *Ann. Entomol. Soc. Am.* 87, 576–582. <https://doi.org/10.1093/aesa/87.5.576>.
- Peterson, C.H., 1985. Patterns of lagoonal bivalve mortality after heavy sedimentation and their paleoecological significance. *Paleobiology* 11, 139–153. <https://doi.org/10.1017/S0094837300011465>.
- Petrulović, J.F., Gutiérrez, P.R., 2016. New basal Odonatoptera (insecta) from the lower carboniferous (Serpukhovian) of Argentina. *Arquivos Entomológicos* 16, 341–358.
- Plint, A.G., 2014. Mud dispersal across a Cretaceous prodelta: storm-generated, wave-enhanced sediment gravity flows inferred from mudstone microtexture and micro-facies. *Sedimentology* 61, 609–647. <https://doi.org/10.1111/sed.12068>.
- Ponomareva, G.Y., Novokshonov, V.G., Naugolnykh, S.V., 1998. Chekarda - Mestonakhzhdenie Permiskikh Iskopaemykh Rasteniy I Nasekomykh (Chekarda – the Locality of Permian Fossil Plants and Insects). Perm State University, Perm, pp. 92.
- Prokop, J., Ren, D., 2007. New significant fossil insects from the upper carboniferous of Ningxia in Northern China. *Eur. J. Entomol.* 104, 267–275. <https://doi.org/10.14411/eje.2007.041>.
- Prokop, J., Pecharová, M., Ren, D., 2016. Hidden surface microstructures on Carboniferous insect *Brodioptera sinensis* (Megasecoptera) enlighten functional morphology and sensorial perception. *Sci. Rep.* 6, 1–11. <https://doi.org/10.1038/srep28316>.
- Robin, N., Béthoux, O., Sidorchuk, E., King, A., Berenguer, F., Ren, D., 2016. A Carboniferous mite on an insect reveals the antiquity of an inconspicuous interaction. *Curr. Biol.* 26, 1–7. <https://doi.org/10.1016/j.cub.2016.03.068>.
- Röhl, H.-J., Schmid-Röhl, A., Oschmann, W., Frimmel, A., Schwark, L., 2001. The Posidonia Shale (Lower Toarcian) of SW-Germany: an oxygen-depleted ecosystem controlled by sea level and paleoclimate. *Palaeogeogr. Palaeoclimatol. Palaeoecol.* 165, 27–52. [https://doi.org/10.1016/S0031-0182\(00\)00152-8](https://doi.org/10.1016/S0031-0182(00)00152-8).
- Rong, Z., Hetland, R.D., Zhang, W., Zhang, X., 2014. Current-wave interaction in the Mississippi-Atchafalaya river plume on the Texas-Louisiana shelf. *Ocean Model.* 84, 67–83.
- Ruan, Y., 1996. North Qilian Mountain-Hexi corridor Subprovince. In: Zhiyi, Z., Dean, W.T. (Eds.), *Phanerozoic Geology of Northwest China*. CRC Press, Boca Raton, pp. 226–228.
- Ruan, Y., Zhou, Z., 1987. Carboniferous cephalopods in Ningxia Hui Autonomous region. In: Bureau of Geology and Mineral Resources. *Namurian Strata and Fossils of Ningxia, China*. Nanjing University Press, Nanjing, pp. 55–177.
- Schieber, J., 1998. Developing a sequence stratigraphic framework for the late Devonian Chattanooga shale of the southeastern US: relevance for the Bakken shale. In: In: Christopher, J.E., Gilboy, C.F., Paterson, D.F., Bend, S.L. (Eds.), *Eights International Williston Basin Symposium, vol. 13*. Saskatchewan Geological Society, Special Publication No., pp. 58–68.
- Schieber, J., Southard, J.B., Schimmelmann, A., 2010. Lenticular shale fabrics resulting from intermittent erosion of water-rich muds – interpreting the rock record in the light of recent flume experiments. *J. Sediment. Res.* 80, 119–128. <https://doi.org/10.2110/jsr.2010.005>.
- Schieber, J., Sur, S., Banerjee, S., 2007. Benthic microbial mats in black shale units from the Vindhyan Supergroup, Middle Proterozoic of India: the challenges of recognizing the genuine article. In: Schieber, J., Bose, P.K., Eriksson, P.G., Banerjee, S., Sarkar, S., Altermann, W., Catuneau, O. (Eds.), *Atlas of Microbial Mat Features Preserved within the Clastic Rock Record*. Elsevier, Amsterdam, pp. 189–197.
- Schieber, J., Yawar, Z., 2009. A new twist on mud deposition – mud ripples in experiment and rock record. *Sediment. Rec.* 7, 4–8. <https://doi.org/10.2110/sedred.2009.2.4>.
- Schmid-Röhl, A., Röhl, H.-J., Oschmann, W., Frimmel, A., Schwark, L., 2002. Paleoenvironmental reconstruction of Lower Toarcian epicontinental black shales (Posidonia Shale, SW Germany): global versus regional control. *Geobios* 35, 13–20. [https://doi.org/10.1016/S0016-6995\(02\)00005-0](https://doi.org/10.1016/S0016-6995(02)00005-0).
- Schneider, J.W., Lucas, S.G., Trümper, S., Stanulla, C., Krainer, K., 2016. Carrizo Arroyo, central New Mexico – a new late Palaeozoic taphotype of arthropod fossiliferous. *N. M. Geol. Soc. Guideb.* 67, 107–116.
- Schöllmann, L., 1999. *Pleurocaris juengeri* n. sp., ein neuer Krebs (Malacostraca, Syncarida) aus dem Namur B von Hagen-Vorhalle (Westfalen, Deutschland). *Geol. Palaontol. Westfalen* 52, 5–17.
- Schultze, H.-P., Maples, C.G., Cunningham, C.R., 1993. The Hamilton Konservat-Lagerstätte: Stephanian terrestrial biota in a marginal-marine setting. *Trans. R. Soc. Edinb. Earth Sci.* 84, 443–451. <https://doi.org/10.1017/S0263593300006246>.
- Shear, W.A., Edgecombe, G.D., 2010. The geological record and phylogeny of the Myriapoda. *Arthropod Struct. Dev.* 39, 174–190. <https://doi.org/10.1016/j.asd.2009.11.002>.
- Shen, S.-Z., Zhang, H., Shang, Q.H., Li, W.-Z., 2006. Permian stratigraphy and correlation of Northeast China: a review. *J. Asian Earth Sci.* 26, 304–326. <https://doi.org/10.1016/j.jseas.2005.07.007>.
- Shi, W., Dong, S., Liu, Y., Hu, J., Chen, X., Chen, P., 2015. Cenozoic tectonic evolution of the South Ningxia region, northeastern Tibetan Plateau inferred from new structural investigations and fault kinematic analysis. *Tectonophysics* 649, 139–164. <https://doi.org/10.1016/j.tecto.2015.02.024>.



- Snigirevskaya, N.S., 1958. Anatomical investigation of fossil leaves (phylloids) of certain Lycopsida in coal balls of Donetz Basin Coalfields (in Russian). *Bot. Zh. Acad. Nauk.* 43, 106–112.
- Sowerby, J., 1812. *The Mineral Conchology of Great Britain; or Coloured Figures and Descriptions of Those Remains of Testaceous Animals or Shells, Which Have Been Preserved at Various Times and Depths in the Earth.* Benjamin Meredith, London, pp. 234.
- Sternberg, K.M., 1821. Versuch einer Geognostisch-Botanischen Darstellung der Flora der Vorwelt. Christoph Ernst Brenck's Wittwe, Regensburg, pp. 33.
- Thrush, S.F., Hewitt, J.E., Cummings, V.J., Elli, J.I., Hatton, C., Lohrer, A., Norkko, A., 2004. Muddy waters: elevating sediment input to coastal and estuarine habitats. *Front. Ecol. Environ.* 2, 299–306. [https://doi.org/10.1890/1540-9295\(2004\)002.\[0299:MWESIT\]2.0.CO;2](https://doi.org/10.1890/1540-9295(2004)002.[0299:MWESIT]2.0.CO;2).
- Tong, Z., 1993. On the relationship between Carboniferous paleogeography and tectonics in the east part of the North Qilian Mountains. *Acta Geol. Gansu* 2, 61–66.
- Tong, Z., Li, H., 1994. Characteristics of Carboniferous lithofacies and paleogeography in eastern part of North Qilian. *Acta Sedimentol. Sin.* 12, 89–97.
- Wang, J., Pfefferkorn, H.W., 2013. The Carboniferous–Permian transition on the North China microcontinent – oceanic climate in the tropics. *Int. J. Coal Geol.* 119, 106–113. <https://doi.org/10.1016/j.coal.2013.07.022>.
- Ward, J.E., MacDonald, B.A., 1996. Pre-ingestive feeding behaviors of two sub-tropical bivalves (*Pinctada imbricata* and *Arca zebra*): responses to an acute increase in suspended sediment concentration. *Bull. Mar. Sci.* 59, 417–432.
- Wei, D., Béthoux, O., Guo, Y., Schneider, J.W., Ren, D., 2013. New data on the singularly 'cockroachoids' from Xiaheyan (Pennsylvanian; Ningxia, China). *Alcheringa* 37, 547–557. <https://doi.org/10.1080/03115518.2013.808863>.
- Westermann, G.E.G., 1996. Ammonoid life and habitat. In: Landman, N.H., Tanabe, K., Davis, R.A. (Eds.), *Ammonoid Paleobiology: from Macroevolution to Palaeogeography.* Springer, Dordrecht, pp. 608–710.
- Wolfe, J.M., Daley, A.C., Legg, D.A., Edgecombe, G.D., 2016. Fossil calibrations for the arthropod tree of life. *Earth Sci. Rev.* 160, 43–110. <https://doi.org/10.1016/j.earscirev.2016.06.008>.
- Xiao, W., Windley, B.F., Allen, M.B., Han, C., 2013. Paleozoic multiple accretionary and collisional tectonics of the Chinese Tianshan orogenic collage. *Gondwana Res.* 23, 1316–1341. <https://doi.org/10.1016/j.gr.2012.01.012>.
- Xie, X., Wang, Y., Shen, H., 2004. Facies analysis and sedimentary environment reconstruction of the late carboniferous in Zhongwei, Ningxia. *Acta Sedimentol. Sin.* 22, 19–28.
- Yan, C.-F., Juan, J.-Y., Zhao, Y.-C., 2008. Lithofacies palaeogeography of the carboniferous in the East of North Qilian Mountains. *Acta Sedimentol. Sin.* 26, 193–201.
- Yang, F., 1987. Early late carboniferous ammonoids from Zhongwei, Ningxia Autonomous region, China. *Geoscience* 1, 157–172.
- Yang, F., 1992. Characteristics of the namurian dysaerobic biofacies from Zhongwei and Zhongning regions, Ningxia, China. *Earth Sci. J. China Univ. Geosci.* 17, 271–279.
- Yang, Q., Gueriau, P., Charbonnier, S., Ren, D., Béthoux, O., 2018. A new tealliocaridid crustacean from the Late Carboniferous of North China and its biogeographic implications. *Acta Palaeontol. Pol.* 63, 111–116. <https://doi.org/10.4202/app.00446.2017>.
- Zhang, P., Burchfiel, B.C., Molnar, P., Zhang, W., Jiao, D., Deng, Q., Wang, Y., Royden, L., 1990. Late cenozoic tectonic evolution of the Ningxia-Hui region, China. *Geol. Soc. Am. Bull.* 102, 1484–1498. [https://doi.org/10.1130/0016-7606\(1990\)102<1484:LCTEOT>2.3](https://doi.org/10.1130/0016-7606(1990)102<1484:LCTEOT>2.3).
- Zhang, Z., Schneider, J.W., Hong, Y., 2013. The most ancient roach (Blattodea): a new genus and species from the earliest Late Carboniferous (Namurian) of China, with discussion of the phylomorphogeny of early blattids. *J. Syst. Palaeontol.* 11, 27–40. <https://doi.org/10.1080/14772019.2011.634443>.
- Zhang, S.-H., Zhao, Y., Song, B., Yang, Z.-Y., Hu, J.-M., Wu, H., 2007. Carboniferous granitic plutons from the northern margin of the North China block: implications for a late Palaeozoic active continental margin. *J. Geol. Soc.* 164, 1–13. <https://doi.org/10.1144/0016-76492005-190>.
- Zheng, R., Wu, T., Zhang, W., Xu, C., Meng, Q., Zhang, Z., 2014. Late Paleozoic subduction system in the northern margin of the Alxa block, Altai: geochronological and geochemical evidences from ophiolites. *Gondwana Res.* 25, 842–858. <https://doi.org/10.1016/j.gr.2013.05.011>.
- Zhu, R., Xu, H., Deng, S., Guo, H., 2007. Lithofacies palaeogeography of the Carboniferous in northern China. *J. Palaeogeogr.* 9, 13–24.